SIAM J. NUMER. ANAL.
Vol. 56, No. 3, pp. 1498–1524

ANALYSIS OF THE PARALLEL SCHWARZ METHOD FOR GROWING CHAINS OF FIXED-SIZED SUBDOMAINS: PART II*

G. CIARAMELLA† AND M. J. GANDER‡

Abstract. According to classical theory, one level Schwarz methods applied to elliptic problems are not scalable in general [A. Toselli and O. Widlund, *Springer Ser. Comput. Math.*, 34, Springer, New York, 2005]. This means that their convergence deteriorates when the number of subdomains increases. In contrast to this classical result, it was observed numerically in [E. Cancès, Y. Maday, and B. Stamm, *J. Chem. Phys.*, 139 (2013), 054111; F. Lipparini, G. Scalmani, L. Lagardère, B. Stamm, E. Cancès, Y. Maday, J.-P. Piquemal, M. J. Frisch, and B. Mennucci, *J. Chem. Phys.*, 141 (2014), 184108; F. Lipparini, B. Stamm, E. Cances, Y. Maday, and B. Mennucci, *J. Chem. Theory Comput.*, 9 (2013), pp. 3637–3648] that in some cases the convergence of the one level Schwarz method does not depend on the number of subdomains. This happens for molecular problems where the domain of definition of the linear elliptic partial differential equation is the union of spherical van der Waal's cavities centered at the atomic position of the molecule. In this case, the computations can naturally be performed using Schwarz methods, where each atom of the molecule corresponds to a subdomain, see [E. Cancès, Y. Maday, and B. Stamm, *J. Chem. Phys.*, 139 (2013), 054111; F. Lipparini, G. Scalmani, L. Lagardère, B. Stamm, E. Cancès, Y. Maday, J.-P. Piquemal, M. J. Frisch, and B. Mennucci, *J. Chem. Phys.*, 141 (2014), 184108; F. Lipparini, B. Stamm, E. Cances, Y. Maday, and B. Mennucci, *J. Chem. Theory Comput.*, 9 (2013), pp. 3637–3648]. We prove here that the scalability results presented in [G. Ciaramella and M. J. Gander, *SIAM J. Numer. Anal.*, 55 (2017), pp. 1330–1356] for a simplified rectangular geometry also hold for realistic two-dimensional chains of circular subdomains. To do so, we first prove some characterization results for the solution of the Laplace equation in the unit disk. Then, using these combined with the maximum principle for harmonic functions, we obtain our convergence theorems for general configurations of molecules. Our convergence results reveal a further very unusual property of the Schwarz method in these simulations: starting from a certain critical overlap size, increasing the overlap further actually decreases the performance of the Schwarz method, in strong contrast to classical Schwarz theory.

Key words. domain decomposition methods, Schwarz methods, chain of atoms, elliptic PDE, Laplace equation, COSMO solvation model

AMS subject classifications. 65N55, 65F10, 65N22, 70-08, 35J05, 35J57

DOI. 10.1137/17M1115885

1. Introduction.

In [6] we analyzed the convergence of the parallel Schwarz method (PSM) for growing chains of fixed-sized rectangular subdomains. This work had been motivated by a series of papers that introduced the so-called ddCOSMO [5, 27, 28], which is an integral equation based implementation of the PSM for the solution of solvation problems, where large molecular systems are involved, and each atom in the molecule corresponds to a subdomain representing the spherical van der Waal's cavity of the corresponding atom. The physical model underlying these solvation processes is the COSMO model presented in [2, 24, 33]. From the numerical analysis viewpoint, the main interest in [5, 27, 28] is scalability results presented by direct numerical experiments: the authors show that the PSM converges in many cases

*Received by the editors February 10, 2017; accepted for publication (in revised form) April 10, 2018; published electronically May 31, 2018.
http://www.siam.org/journals/sinum/56-3/M111588.html
Funding: The work of the authors was supported by Swiss National Science Foundation (SNSF) projects PASC-DIAPHANE and 200020_149107/1.
†Fachbereich Mathematik und Statistik, Universität Konstanz, Konstanz D-78457, Germany (gabriele.ciaramella@uni-konstanz.de).
‡Section de Mathématiques, University of Geneva, Geneva CH-1211, Switzerland (martin.gander @unige.ch).

independently of the number of atoms (subdomains) in the molecules. This unusual behavior of the one-level PSM motivated our work [6], where we proved the scalability result for a simplified, rectangular approximation of a linear chain of subdomains.

The present paper is the sequel of [6]: our goal is to prove that ddCOSMO is indeed scalable in many realistic geometrical settings of molecular chains of subdomains. In particular, we focus on two-dimensional structure (chains) composed by intersecting disks (subdomains) mimicking in $\mathbb{R}^2$ the real situation of linear molecules. To analyze the convergence of the PSM in this more realistic geometric setting, we rely on techniques based on the maximum principle and conformal mappings. We obtain three main new results: first, we prove that the PSM for growing chains of fixed-sized subdomains converges geometrically and, in many cases, independently of the number of subdomains. Second, in order to prove these convergence results, some characterizations of the solution of Laplace boundary value problems are needed. In particular, we show that the solution of the Laplace boundary value problem in the half-plane and in the unit disk, for a unit-step boundary condition, is constant on arcs of circles. And finally, the third novelty we prove is that for these simulations, increasing the overlap beyond a certain size in the Schwarz method actually decreases the performance of the method, which is in contrast to classical Schwarz theory for Laplace type problems. The geometry therefore can have an important influence on the performance of the Schwarz method, a research area which has only recently been paid more attention to (see, e.g., [11, 15, 3, 17, 16, 18, 34, 19]), and the surprising overlap behavior is completely new. Note that also the discretization can have a strong influence on the performance of the Schwarz method, which was first pointed out in [8]. This is particularly true for discontinuous Galerkin discretizations of Schwarz methods; see [12, 4, 13, 21, 14].

Our paper is organized as follows. In section 2, we introduce a classification of two-dimensional chains of atoms and define the PSM for their solution. Section 3 focuses on the characterization of the solutions of the Laplace boundary value problems in the half-plane and in the unit disc. In section 4, we prove our main convergence results: we show that the PSM converges geometrically and independently of the number of subdomains for general linear chains. Our analysis is at the continuous level, in contrast to the classical abstract Schwarz framework [32]; for an exception defining and studying the abstract Schwarz framework at the continuous level, see [15, 16]. In section 5, we use the results obtained in section 4 to prove convergence independently of the number of subdomains for several relevant geometric configurations of the two-dimensional analogue of molecules, and also that increasing the overlap beyond a specific size decreases the performance of the Schwarz method applied to chains of subdomains, in contrast to classical Schwarz theory. These results are supported by numerical experiments based on finite-element discretizations. We present our conclusions in section 6.

2. Parallel Schwarz method for chains of atoms. We consider the problem of a chain of N atoms whose states u_j are defined on circular subdomains. Each subdomain Ω_j is a ball in $\mathbb{R}^2$ that intersects other subdomains Ω_k such that the entire problem is defined over $\Omega = \cup_{j=1}^{N} \Omega_j$. In particular, we focus on "chains" or "ensembles" of subdomains that we classify as follows.

DEFINITION 1 (chain of subdomains). *A set of a finite number N of subdomains, where each subdomain is an open ball $\Omega_j \subset \mathbb{R}^2$ for $j = 1, \ldots, N$, is said to be a chain and denoted by $\mathcal{C}$ if and only if the domain of the chain, defined as $\Omega := \cup_{j=1}^{N} \Omega_j$, is a path connected set. We say that the chain $\mathcal{C}$ is a*

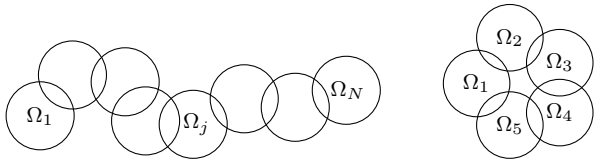

FIG. 1. *Example of a linear chain (left) and a ringed chain (right).*

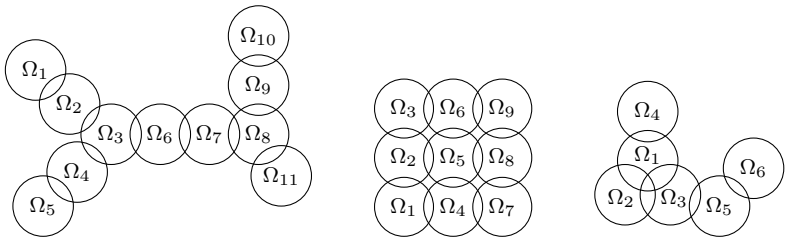

FIG. 2. *Examples of a branched chain (left), a meshed chain (middle), and a branched chain (right) that does not satisfy* (1).

- *"linear chain" (see Figure* 1 *(left)) if* $\Omega_j \cap \Omega_{j\pm1} \neq \emptyset$, $\overline{\Omega}_j \cap \overline{\Omega}_{j\pm k} = \emptyset$ *for* $k > 1$, *and* $\Omega_1 \cap \Omega_j \neq \emptyset$ *if and only if* $j = 2$ *and* $\Omega_N \cap \Omega_j \neq \emptyset$ *if and only if* $j = N-1$*;*
- *"ringed chain" (see Figure* 1 *(right)) if* $\Omega_j \cap \Omega_{j\pm1} \neq \emptyset$, $\overline{\Omega}_j \cap \overline{\Omega}_{j\pm k} = \emptyset$ *for* $k > 1$, *and* $\Omega_1 \cap \Omega_N \neq \emptyset$*;*
- *"branched chain" (see Figure* 2 *(left)) if* $\mathcal{C}$ *can be decomposed into subchains* $\mathcal{C}_\ell$ *such that* $\cup_\ell \mathcal{C}_\ell = \mathcal{C}$, *where each subchain* $\mathcal{C}_\ell$ *is a linear chain or a ringed chain and the intersection of any two subchains is an empty set or a singleton; in the latter case, the unique element (subdomain) in the intersection is said to be a "connection subdomain";*[1]
- *"meshed chain" (see Figure* 2 *(middle)) if the centers of the subdomains* Ω_j *in* $\mathcal{C}$ *are distributed on a grid.*

Linear chains satisfy the following two conditions: for all distinct $j, k, \ell \in \{1, \ldots, N\}$ we have

$$\overline{\Omega}_j \cap \overline{\Omega}_k \cap \overline{\Omega}_\ell = \emptyset, \tag{1a}$$

$$\text{if } \Omega_j \cap \Omega_k \neq \emptyset \text{ and } \Omega_k \cap \Omega_\ell \neq \emptyset, \text{ then } \Omega_j \cap \Omega_\ell = \emptyset. \tag{1b}$$

These conditions were also assumed by Lions in [25] to ensure a variational interpretation of the Schwarz method. For example, the chain on the right in Figure 2 does not satisfy (1) because of the atoms Ω_1, Ω_2, and Ω_3, whose intersection is nonempty. Note that in general, (1a) and (1b) are not equivalent: an example is given in Figure 3 (left), where only (1a) is satisfied. Note also that ringed, branched, and meshed chains do not necessarily satisfy (1). The results presented in this paper are valid for chains of atoms that satisfy (1a). Furthermore, we also assume (1b) for some of our results.

DEFINITION 2 (equidistant chain of subdomains). *Consider a chain* $\mathcal{C}$ *of* N *subdomains such that the* Ω_j *are unit balls. Let* Ω_j *and* Ω_k *be any two subdomains in* $\mathcal{C}$ *such that* $\Omega_j \cap \Omega_k \neq \emptyset$ *and denote by* $d_{j,k} \in \mathbb{R}^+$ *the distance between the center of*

[1] The branched chain on the left in Figure 2 can, for example, be decomposed into the subchains $\mathcal{C}_1 = \{\Omega_1, \Omega_2, \Omega_3\}$, $\mathcal{C}_2 = \{\Omega_3, \Omega_4, \Omega_5\}$, $\mathcal{C}_3 = \{\Omega_3, \Omega_6, \Omega_7, \Omega_8\}$, $\mathcal{C}_4 = \{\Omega_8, \Omega_{11}\}$, and $\mathcal{C}_5 = \{\Omega_8, \Omega_9, \Omega_{10}\}$, where Ω_3 and Ω_8 are connection subdomains.

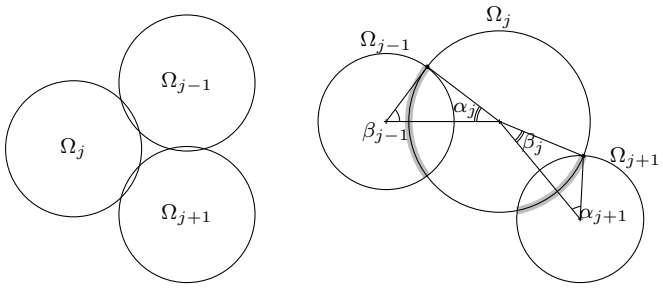

FIG. 3. *Left: example of a chain of atoms where* (1a) *is satisfied but* (1b) *is not. Right: details for circular subdomains.*

Ω_j *and* Ω_k. *We say that the chain* $\mathcal{C}$ *is equidistant if* $d_{j,k} = d_{n,m}$ *for any* $j,k,n,m \in \{1,\dots,N\}$ *such that* $\Omega_j \cap \Omega_k \neq \emptyset$ *and* $\Omega_n \cap \Omega_m \neq \emptyset$.

We show in Figure 3 (right) details for circular subdomains: if the subdomains Ω_j are disks of equal radius and equidistant as for an equidistant chain of subdomains, then $\alpha_j = \alpha_{j+1} = \beta_j = \beta_{j-1}$.

Now, for $j = 1,\dots,N$, we define the index sets $\mathcal{I}_j := \{k : 1 \le k \le N\,;\, k \neq j,\ \text{and } \Omega_j \cap \Omega_k \neq \emptyset\}$. With this notation, the state $u_j(x,y)$ of the jth subdomain is the solution to

$$\begin{aligned} -\Delta u_j &= f_j \ \text{ in } \Omega_j, \\ u_j &= u_k \ \text{in } \partial\Omega_j \cap \Omega_k \ \forall k \in \mathcal{I}_j, \\ u_j &= g_j \ \text{ on } \Gamma_{j,0} := \partial\Omega_j \setminus \bigcup_{k\in\mathcal{I}_j} \big(\Omega_k \cap \partial\Omega_j\big). \end{aligned} \tag{2}$$

Notice that the entire chain problem is

$$\begin{aligned} -\Delta u &= f \quad \text{in } \Omega, \\ u &= g \quad \text{on } \partial\Omega, \end{aligned} \tag{3}$$

and the functions u_j, f_j, and g_j are the restrictions of u, f, and g to Ω_j and $\partial\Omega_j$. We assume that g is continuous on the boundary, that is, $g \in C(\partial\Omega)$. The function f is assumed sufficiently regular to guarantee that there exists a unique classical solution of (3), that is, $u \in C^2(\Omega) \cap C(\overline{\Omega})$. Notice that, since Ω is a domain in $\mathbb{R}^2$ and the boundary $\partial\Omega$ is composed by a finite number of simple curves, if f is bounded and locally Hölder continuous, then the unique solution of (3) is a classical solution $u \in C^2(\Omega) \cap C(\overline{\Omega})$ [20, Theorem 2.14, discussion p. 26, Theorem 4.3]; see also [7, p. 343] and [9, section 2.2.3] for further discussions.

As in [5] the PSM for the solution of (2)–(3) is

$$\begin{aligned} -\Delta u_j^n &= f_j \ \text{ in } \Omega_j, \\ u_j^n &= g_j^n \ \text{ on } \partial\Omega_j, \end{aligned} \tag{4}$$

where

$$g_j^n = \begin{cases} g_j & \text{on } \Gamma_{j,0}, \\ u_k^{n-1} & \text{on } \partial\Omega_j \cap \overline{\Omega}_k \ \forall k \in \mathcal{I}_j. \end{cases} \tag{5}$$

We assume that u_j^0 is in $C(\overline{\Omega}_j)$ and $u_j^0 = g_j$ on $\Gamma_{j,0}$ for all j. Recalling that $g \in C(\partial\Omega)$ and f is assumed sufficiently regular, it is easy to see that for $n = 1$ the boundary condition for the jth problem is

$$g_j^1 = \begin{cases} g_j & \text{on } \Gamma_{j,0}, \\ u_k^0 & \text{on } \partial\Omega_j \cap \overline{\Omega}_k \, \forall k \in \mathcal{I}_1, \end{cases}$$

which is continuous, that is, $g_j^1 \in C(\partial\Omega_j)$. This implies that $u_j^1 \in C^2(\Omega_j) \cap C(\overline{\Omega}_j)$. Therefore, one can repeat this argument for $n = 2, 3, \ldots$ to obtain that $g_j^n \in C(\partial\Omega_j)$ and hence that $u_j^n \in C^2(\Omega_j) \cap C(\overline{\Omega}_j)$ for all j.

Next, we denote the error at each iteration n by $e_j^n := u_j - u_j^n$. Hence, the PSM (4) can be written in terms of the error e_j^n:

$$\begin{aligned} -\Delta e_j^n &= 0 \quad \text{in } \Omega_j, \\ e_j^n &= 0 \quad \text{on } \Gamma_{j,0}, \\ e_j^n &= e_k^{n-1} \text{ on } \partial\Omega_j \cap \overline{\Omega}_k \quad \forall k \in \mathcal{I}_j. \end{aligned} \tag{6}$$

In what follows, we analyze the convergence of the PSM (6): our goal is to prove that the sequence $\{e_j^n\}_n$ converges to zero geometrically and independently of the number of subdomains N. Moreover, we are interested in a direct estimate of the convergence factor governing the convergence behavior.

3. Characterization of the solution to the Laplace problem. We first study the Laplace equation on the right-half-plane with a unit-step function as boundary condition on the y-axis and prove that the solution is constant on arcs of circles (Theorem 4). We then show that a similar result also holds on a disk (Theorem 5), and we give a specific estimate for the case where the boundary condition is a piecewise-constant function (Theorem 6). To do so, we will use the Poisson kernel of the disk and the half-space, respectively; see, e.g., [1, 9, 29, 31]:

$$P_r(\varphi) = \frac{1}{2\pi} \frac{1 - r^2}{1 - 2r\cos(\varphi) + r^2} \quad \text{and} \quad P_x(y) = \frac{1}{\pi} \frac{x}{x^2 + y^2}. \tag{7}$$

3.1. The Laplace equation in the half-plane. We begin by studying

$$\begin{aligned} -\Delta v &= 0 \quad \text{in } \mathbb{R}^+ \times \mathbb{R}, \\ v(0, y) &= 1 \quad \text{for } y \in [-a, a], \\ v(0, y) &= 0 \quad \text{for } y \in \mathbb{R} \setminus [-a, a], \\ \lim_{r \to \infty} v(x, y) &= 0 \quad \text{with } r = \sqrt{x^2 + y^2}, \end{aligned} \tag{8}$$

where $a > 0$ is an arbitrary given number. The following lemma shows that the solution of (8) is constant along arcs of circles.

LEMMA 3. *Let $B_r^a(0, d)$ and $B_\ell^a(0, -d)$ be two balls in $\mathbb{R}^2$ passing through the points $(0, a)$ and $(0, -a)$ and centered at $(0, d)$ and $(0, -d)$ with $d \geq 0$ as illustrated in Figure 4. Then for any (x, y) lying on the arcs*

$$\mathcal{C}_d^r(a) := \big(\mathbb{R}^+ \times \mathbb{R}\big) \cap \partial B_r^a(0, d) \quad \textit{and} \quad \mathcal{C}_d^\ell(a) := \big(\mathbb{R}^+ \times \mathbb{R}\big) \cap \partial B_\ell^a(0, -d),$$

the solution of (8) satisfies

$$v(x, y) = \frac{1}{2} \mp \frac{1}{\pi} \arctan\left(\frac{d}{a}\right). \tag{9}$$

The sign in (9) is negative if $(x, y) \in \mathcal{C}_d^r(a)$ (Figure 4, right) and positive if $(x, y) \in \mathcal{C}_d^\ell(a)$ (Figure 4, left).

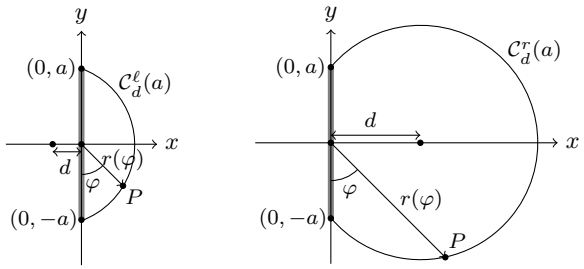

FIG. 4. *Left: the center of the circle is on the left of the origin ($\mathcal{C}_d^\ell(a)$). Right: the center of the circle is on the right of the origin ($\mathcal{C}_d^r(a)$).*

Proof. The solution of (8) can be expressed using the Poisson kernel (7),

$$v(x,y) = \int_{-a}^{a} P_x(y-t)dt. \tag{10}$$

Notice that since the boundary condition is a step function and in $L^p(\mathbb{R})$, v is in $C^2(\mathbb{R}^+ \times \mathbb{R})$ and harmonic in $\mathbb{R}^+ \times \mathbb{R}$; see, e.g., [1, 31] and references therein. Integrating (10) we obtain

$$v(x,y) = \frac{1}{\pi}\left[\arctan\left(\frac{y+a}{x}\right) - \arctan\left(\frac{y-a}{x}\right)\right]. \tag{11}$$

Recall that for any $w, z \in \mathbb{R}$ we have

(12)
$$\arctan(w) + \arctan(z) = \arctan\Big(\frac{w+z}{1-wz}\Big) \text{ if } -\frac{\pi}{2} < \arctan(w) + \arctan(z) < \frac{\pi}{2},$$

(13)
$$\arctan(w) + \arctan(z) = \pi + \arctan\left(\frac{w+z}{1-wz}\right) \text{ if } \frac{\pi}{2} < \arctan(w) + \arctan(z) < \pi.$$

In the case (12), we obtain for (11)

$$v(x,y) = \frac{1}{\pi}\arctan\left(\frac{2xa}{x^2+y^2-a^2}\right). \tag{14}$$

In polar coordinates, $x = r\sin\varphi$ and $y = r\cos\varphi$, the solution (14) becomes

$$v(r,\varphi) = \frac{1}{\pi}\arctan\left(\frac{2ra\sin\varphi}{r^2-a^2}\right). \tag{15}$$

Consider a point P lying on $\mathcal{C}_d^r(a)$ (Figure 4, right). The position of P in polar coordinates is given by $(r(\varphi),\varphi)$ such that $r(\varphi) = d\sin\varphi + \sqrt{a^2 + (d\sin\varphi)^2}$. By replacing this into (15) we get

$$\begin{aligned} v(r(\varphi),\varphi) &= \frac{1}{\pi}\arctan\left(\frac{2r(\varphi)a\sin\varphi}{r(\varphi)^2-a^2}\right) \\ &= \frac{1}{\pi}\arctan\left(\frac{2\left(d\sin\varphi + \sqrt{a^2+(d\sin\varphi)^2}\right)a\sin\varphi}{\left(d\sin\varphi + \sqrt{a^2+(d\sin\varphi)^2}\right)^2 - a^2}\right) \end{aligned}$$

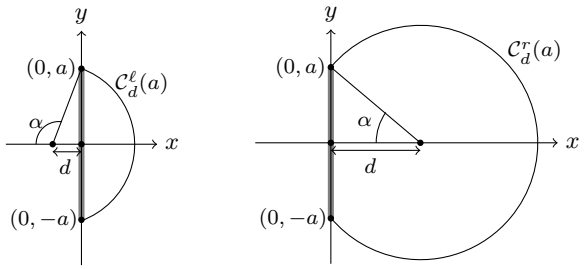

FIG. 5. *Left: the center of the circle is on the left of the origin ($d < 0$; $\mathcal{C}_d^\ell(a)$). Right: the center of the circle is on the right of the origin ($d \geq 0$; $\mathcal{C}_d^r(a)$).*

$$= \frac{1}{\pi} \arctan\left(\frac{2\left(d\sin\varphi + \sqrt{a^2 + (d\sin\varphi)^2}\right) a \sin\varphi}{2d\sin\varphi\left(d\sin\varphi + \sqrt{a^2 + (d\sin\varphi)^2}\right)} \right)$$

$$= \frac{1}{\pi} \arctan\left(\frac{a}{d}\right) = \frac{1}{\pi}\left[\frac{\pi}{2} - \arctan\left(\frac{d}{a}\right)\right], \tag{16}$$

where we used (12). Therefore, (16) is valid only in the case that $-\frac{\pi}{2} < \frac{\pi}{2} - \arctan(\frac{d}{a}) < \frac{\pi}{2}$. This is satisfied since $v(r(\varphi), \varphi) = \frac{1}{2}$ for $d = 0$ and $v(r(\varphi), \varphi) \to 0$ as $d \to \infty$.

Next, consider that P lies on $\mathcal{C}_d^\ell(a)$ (Figure 4, left). In this case we have that $r(\varphi) = -d\sin\varphi + \sqrt{a^2 + (d\sin\varphi)^2}$. Recall that the solution v is in $C^2(\mathbb{R}^+ \times \mathbb{R})$ and $v(r(\varphi), \varphi) = \frac{1}{2}$ for $d = 0$ as we just have seen. By the maximum principle [1, 9] we have that $\frac{1}{2} \leq v(r(\varphi), \varphi) \leq 1$. Therefore, we must use (13) and obtain with a similar argument as in (16)

$$v(r(\varphi), \varphi) = \frac{1}{\pi}\left[\frac{\pi}{2} + \arctan\left(\frac{d}{a}\right)\right],$$

which completes our proof. ∎

THEOREM 4. *The solution $v(x, y)$ of the half-space problem* (8) *satisfies for any $(x, y) \in \mathcal{C}_d^r(a)$ or $(x, y) \in \mathcal{C}_d^\ell(a)$*

$$v(x, y) = \frac{\alpha}{\pi}, \tag{17}$$

where α identifies $\mathcal{C}_d^r(a)$ or $\mathcal{C}_d^\ell(a)$ and is defined as the angle between the x-axis and the line that connects the center of the circle with the point $(0, a)$; see Figure 5.

Proof. We recall from Lemma 3 that $v(x, y) = [\frac{1}{2} \mp \frac{1}{\pi}\arctan(\frac{d}{a})]$. Notice that in Lemma 3, in order to deal with the shift of the arctan function, we worked with a distance $d \geq 0$. Next, we allow d to assume negative values. In this way $d \geq 0$ generates the arc $\mathcal{C}_d^r(a)$ (Figure 5, right), while $d < 0$ generates $\mathcal{C}_d^\ell(a)$ (Figure 5, left). The solution v, which is continuous, can then be expressed without sign distinction,

$$v(x, y) = \left[\frac{1}{2} - \frac{1}{\pi}\arctan\left(\frac{d}{a}\right)\right].$$

Now, we notice that $\frac{a}{d} = \tan(\alpha)$ (see Figure 5) and we conclude by

$$v(x, y) = \left[\frac{1}{2} - \frac{1}{\pi}\arctan\left(\frac{1}{\tan\alpha}\right)\right] = \left[\frac{1}{2} - \frac{1}{\pi}\left(\frac{\pi}{2} - \arctan\left(\tan\alpha\right)\right)\right] = \frac{\alpha}{\pi}. \qquad \blacksquare$$

We used in (8) as boundary condition $v(0,y) = 1$ on $[-a,a]$, but we could have used any other constant C, and by linearity Theorem 4 would still hold with $v(x,y) = C\frac{\alpha}{\pi}$.

3.2. The Laplace equation on a disk. We now focus on the problem posed on the disk shown in Figure 6 with a unit-step boundary condition,

$$
\begin{aligned}
-\partial_{rr}w - \frac{1}{r}\partial_r w - \frac{1}{r^2}\partial_{\varphi\varphi} w = 0 \ \text{ in } \Omega,\\
w(r,\varphi) = w(r, 2\pi + \varphi),\\
w(1,\varphi) = 1 \ \text{ for } \varphi \in [\pi - \alpha, \pi + \alpha],\\
w(1,\varphi) = 0 \ \text{ for } \varphi \in [-\pi - \alpha, \pi - \alpha].
\end{aligned} \tag{18}
$$

We first prove using conformal mappings that the solution w is constant on arcs of circles.

THEOREM 5. *Problem* (18) *has a unique solution* $w \in C^2(\Omega)$ *which is constant on arcs of circles* $\mathcal{A}_{\widetilde{\alpha}}$ *parametrized by angles* $\widetilde{\alpha}$ *between the* x*-axis and the line that connects the center of the arc* $\mathcal{A}_{\widetilde{\alpha}}$ *to the point* $(0,a)$ *(see Figure* 7*), i.e.,*

$$
w(r,\varphi) = \frac{\widetilde{\alpha} - \alpha}{\pi} \quad \forall (r,\varphi) \in \mathcal{A}_{\widetilde{\alpha}} \tag{19}
$$

with $0 < w(x,y) < 1$ *for any* $(x,y) \in \Omega$ *and* $\alpha \le \widetilde{\alpha} < \pi$.

Proof. Recall Theorem 4 and consider Figure 8. Denote by P the intersection of the arc $\mathcal{C}_d^r(a)$ with the (positive) y-axis, that is, $P = (0,a)$. Denote by $\mathcal{L}_1$ the y-axis

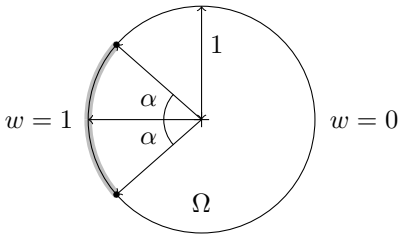

FIG. 6. *Laplace boundary value problem on the unit disk. The angle* α *parametrizes the arc corresponding to the boundary condition* $w = 1$.

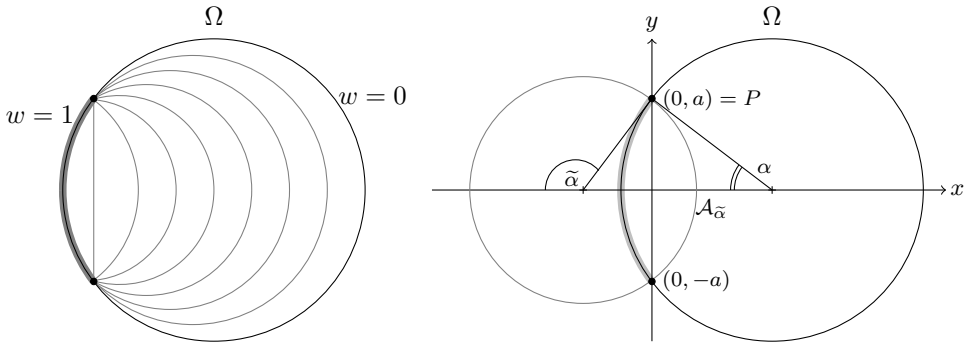

FIG. 7. *Left: level sets of* w. *Right: geometric parametrization of a level set of* w.

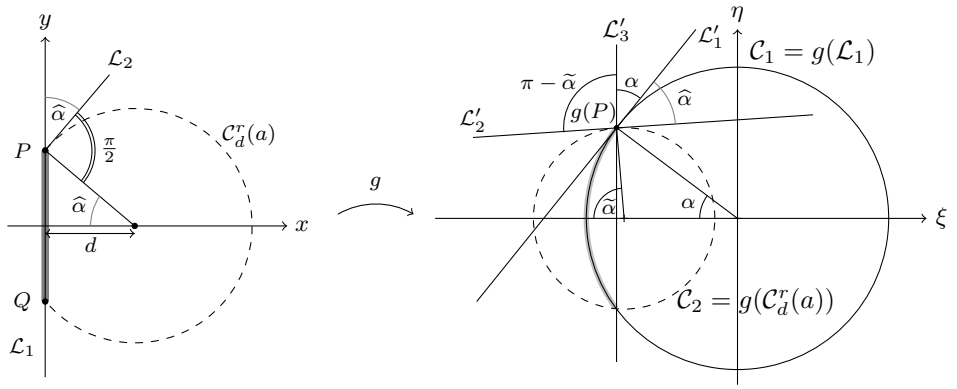

FIG. 8. *Geometry of the mapping of the right-half-plane with an arc $\mathcal{C}_d^r(a)$ (left) onto a disk (right). Notice that the arc $\mathcal{C}_d^r(a)$ is mapped to the arc C_2 and the segment $\overline{PQ}$ (in gray) is mapped to an arc $g(\overline{PQ})$ (in gray).*

and by $\mathcal{L}_2$ the straight line passing through P and tangent to $\mathcal{C}_d^r(a)$ (see Figure 8 on the left). We denote by $\widehat{\alpha}$ the angle between $\mathcal{L}_1$ and $\mathcal{L}_2$ and notice that $\widehat{\alpha}$ is also the angle formed by the x-axis and the segment that connects the center of $\mathcal{C}_d^r(a)$ with P. Hence, by Theorem 4 the solution $v(x, y)$ of the Laplace problem (8) is constant on $\mathcal{C}_d^r(a)$ and has the value $\frac{\widehat{\alpha}}{\pi}$. We now introduce a change of variables using a conformal map $g : (x, y) \mapsto (\xi, \eta)$ and denote by $w(\xi, \eta) := v(g^{-1}(\xi, \eta))$ with nonzero Jacobian g'. This change of variables leads also to a transformed equation (8), namely,

$$\Delta_{(x,y)} v = |g'(x, y)|^2 \Delta_{(\xi,\eta)} w = 0, \tag{20}$$

where $\Delta_{(x,y)}$ and $\Delta_{(\xi,\eta)}$ are the Laplace operators in the coordinates (x, y) and (ξ, η); see, e.g., [22, section 5.9] and [30, section 6]. Well-known examples of conformal maps are Möbius transformations, which map generalized circles (circles and lines in the complex plane) to generalized circles; see, e.g., [22, Theorem 5.3b]. In particular, we consider the Möbius transformation $(x, y) \mapsto g(x, y) =: (\xi, \eta)$ given by (see [30, Example 6.3])

$$g(x, y) = \left(\frac{x^2 + y^2 - 1}{(x + 1)^2 + y^2}\,,\ \frac{2y}{(x + 1)^2 + y^2} \right).$$

This transformation has the property to map the right-half-plane onto the unit disk, and since the function $w(\xi, \eta) := v(g^{-1}(\xi, \eta))$ satisfies (20) and thus $\Delta_{(\xi,\eta)} w = 0$, it solves the boundary value problem (18). Moreover, a direct calculation shows that the function g maps the arc $\mathcal{C}_d^r(a)$ onto the arc $\mathcal{C}_2 := g(\mathcal{C}_d^r(a))$ lying inside the unit disk. Hence, w is constant on $\mathcal{C}_2$ and has the value $w|_{\mathcal{C}_2} = \frac{\widehat{\alpha}}{\pi}$.

Now, denote by α the angle between the ξ-axis and the segment that connects the origin (center of $\mathcal{C}_1$) with the point $g(P)$ and by $\widetilde{\alpha}$ the angle that connects the center of $\mathcal{C}_2$ with $g(P)$. We want to show that $\widehat{\alpha} = \widetilde{\alpha} - \alpha$. To do so, notice that $\mathcal{C}_2$ intersects $\mathcal{C}_1$ in $g(P)$. Denote by $\mathcal{L}_1'$ and $\mathcal{L}_2'$ the straight lines tangent to $\mathcal{C}_1$ and $\mathcal{C}_2$ at $g(P)$. Since the Möbius transformation g is conformal, it preserves angles. Hence, the angle between $\mathcal{L}_1'$ and $\mathcal{L}_2'$ equals $\widehat{\alpha}$ (see Figure 8).

Now, denote by $\mathcal{L}_3'$ the straight line passing through the two points in which $\mathcal{C}_1$ and $\mathcal{C}_2$ intersect. Then it is easy to see that the angle between the η-axis and $\mathcal{L}_1'$ is equal to α. Moreover, the angle between the η-axis and $\mathcal{L}_2'$ is equal to $\pi - \widetilde{\alpha}$ (see Figure 8), and hence

$$\widehat{\alpha} = \pi - (\pi - \widetilde{\alpha}) - \alpha = \widetilde{\alpha} - \alpha.$$

Therefore, the value of the solution of (18) on $\mathcal{C}_2$ is given by $w|_{\mathcal{C}_2} = \frac{\widehat{\alpha}}{\pi} = \frac{\widetilde{\alpha}-\alpha}{\pi}$, which completes our proof. ∎

Notice that the previous theorem allows us to recover an important result that characterizes the behavior of the solution to Laplace boundary value problems near boundary points where the boundary condition has a jump discontinuity. In fact, one can easily see that $\lim_{\mathcal{C}_2 \ni (x,y) \to g(P)} v(x,y) = \frac{\widetilde{\alpha}-\alpha}{\pi} = \frac{\theta}{\pi}$, where $\theta := \widetilde{\alpha} - \alpha$ is the angle between $\partial\Omega$ and the curve $\mathcal{C}_2$. This result is stated in [26, p. 54] and the corresponding proof can be found in [23, p. 633].

We can now obtain the main bound for the Laplace solution corresponding to a piecewise constant periodic function, which will allow us to prove a sharp convergence estimate for the PSM.

THEOREM 6. *Consider the domain $\Omega := B_1(0,d)$ and denote by $\partial\Omega$ the corresponding boundary. Let Γ_ℓ and Γ_r be two closed and connected subsets of $\partial\Omega$ such that $\Gamma_\ell \cap \Gamma_r = \emptyset$. Consider the Laplace boundary value problem*

$$\begin{aligned} -\Delta w &= 0 \ \text{ in } \Omega, \\ w &= 1 \ \text{ on } \Gamma_\ell \text{ and } \Gamma_r, \\ w &= 0 \ \text{ on } \partial\Omega \setminus (\Gamma_\ell \cup \Gamma_r)\,. \end{aligned} \tag{21}$$

Denote by $\mathcal{A}^\ell_{\widetilde{\alpha}}$ the arc passing through the extrema O_1 and O_2 of Γ_ℓ characterized by the angle α and parametrized by $\widetilde{\alpha}$ as in Figure 9. Then the solution w to problem (21) on $\mathcal{A}^\ell_{\widetilde{\alpha}}$, that is, $w|_{\mathcal{A}^\ell_{\widetilde{\alpha}}}$, is positive ($w|_{\mathcal{A}^\ell_{\widetilde{\alpha}}} > 0$) and admits a unique maximum located at the (unique) point $O_3 \in \mathcal{A}^\ell_{\widetilde{\alpha}} \cap \mathcal{A}^r_{\widetilde{\beta}}$, where $\mathcal{A}^r_{\widetilde{\beta}}$ is the unique arc of circle passing through the extrema O_4 and O_5 of Γ_r and touching $\mathcal{A}^\ell_{\widetilde{\alpha}}$ at O_3, characterized by the angles β and $\widetilde{\beta}$. Moreover, we have that

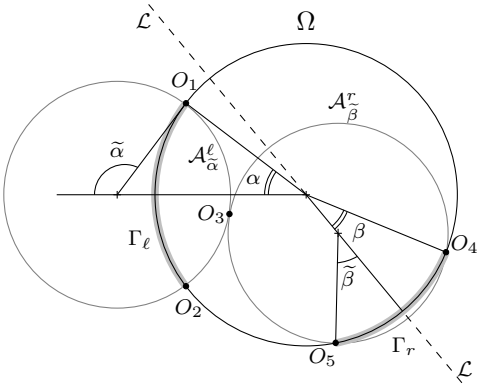

FIG. 9. *Geometric representation of problem (21). This figure shows the domain Ω and its boundary, where the gray solid-thick lines represent Γ_ℓ and Γ_r. The two gray circles are the ones on which the two arcs $\mathcal{A}^\ell_{\widetilde{\alpha}}$ and $\mathcal{A}^r_{\widetilde{\beta}}$ lie. The points O_1, O_2, O_4, and O_5 are the extrema of Γ_ℓ and Γ_r. The straight line $\mathcal{L}$ bisects the segment $\overline{O_4O_5}$ and hence represents the set of points on which the center of the arc $\mathcal{A}^r_{\widetilde{\beta}}$ lies. The point O_3 is the point where $\mathcal{A}^\ell_{\widetilde{\alpha}}$ and $\mathcal{A}^r_{\widetilde{\beta}}$ touch and represents the (unique) maximum point of $w|_{\mathcal{A}^\ell_{\widetilde{\alpha}}}$.*

$$w(O_3) = \frac{\widetilde{\alpha} + \widetilde{\beta} - \alpha - \beta}{\pi}, \tag{22}$$

and $0 < w(O_3) < 1$.

Proof. By linearity of problem (21) the unique solution w can be obtained as $w(O) = w_\ell(O) + w_r(O)$ for all $O \in \Omega$, where w_ℓ and w_r solve

$$\begin{aligned} -\Delta w_\ell &= 0 \text{ in } \Omega, & & & -\Delta w_r &= 0 \quad \text{in } \Omega, \\ w_\ell &= 1 \text{ on } \Gamma_\ell & & \text{and} & w_r &= 1 \quad \text{on } \Gamma_r, \\ w_\ell &= 0 \text{ on } \partial\Omega \setminus \Gamma_\ell, & & & w_r &= 0 \quad \text{on } \partial\Omega \setminus \Gamma_r. \end{aligned}$$

Therefore, we can invoke Theorem 5 for both w_ℓ and w_r and use the fact that w_ℓ and w_r are constant on all the arcs passing through the extrema of Γ_ℓ and Γ_r. Consider the arc $\mathcal{A}^\ell_{\widetilde{\alpha}}$. We look for the arc $\mathcal{A}$ passing through O_4 and O_5 that intersects $\mathcal{A}^\ell_{\widetilde{\alpha}}$ and such that the value of $w_r|_{\mathcal{A}}$ is maximum. It is clear from Theorem 5 that the arc $\mathcal{A}$ is the one touching $\mathcal{A}^\ell_{\widetilde{\alpha}}$ tangentially and corresponding to the angle $\widetilde{\beta}$ (Figure 9). Since there exists a unique circle passing through three given noncollinear points, $\mathcal{A}$ coincides with $\mathcal{A}^r_{\widetilde{\beta}}$. It follows that in O_3 we have

$$w(O_3) = w_\ell(O_3) + w_r(O_3) = \frac{\widetilde{\alpha} - \alpha}{\pi} + \frac{\widetilde{\beta} - \beta}{\pi},$$

where we used again Theorem 5. Finally, standard arguments, like [26, section 2, Lemma 3] and the maximum principle for harmonic functions [1, section 1, Theorem 1.2.4], imply that $0 < w(O) < 1$ for any $O \in \Omega$. ∎

The results given in Theorems 5 and 6 are presented for Ω equal to the unit ball, but remain valid for balls of any radius. In Theorem 6 we invoked standard arguments, that are [26, section 2, Lemma 3] and [1, section 1, Theorem 1.2.4], to prove that the quantity $w(O_3) = \frac{\widetilde{\alpha}-\alpha+\widetilde{\beta}-\beta}{\pi}$ satisfies $0 < w(O_3) < 1$. These arguments are very powerful techniques. However, they do not provide any information on the dependence of $w(O_3)$ on β and hence on the arc Γ_r. Notice that $\widetilde{\beta}$ depends nonlinearly on β and α. A direct calculation, even if cumbersome, can show the same result and provide more information on the behavior of $w(O_3)$ with respect to β. Some examples are provided in sections 4 and 5.

4. Convergence analysis of the parallel Schwarz method. In this section, we analyze the convergence of the PSM (4)–(6) for the solution of chains of subdomains. We prove in Theorem 7 that the PSM for a chain of atoms converges geometrically. Corollary 8 states that the convergence of the PSM for an equidistant chain of collinear subdomains (unit balls) converges independently of the number of subdomains. In Theorem 11, we prove that the PSM for the solution of any equidistant linear chain converges independently of the number of subdomains (subdomains). The results presented in this section can be used to prove convergence of the PSM (independently of the number of subdomains) for more general ringed, branched, and meshed chains. Several representative examples are given in section 5.

Our first result is Theorem 7, which is proved in the same spirit as in [26].

THEOREM 7. *Consider a chain $\mathcal{C}$ of N subdomains (not necessarily equidistant) such that* (1a) *holds. Denote by e_j^n the solution to problem* (6) *at the nth iteration of the PSM initialized by $e_j^0 \in C(\overline{\Omega}_j)$. Then we have that*

$$\max_{j\in\mathcal{I}} \|e_j^n\|_{C(\partial\Omega_j)} \le \rho \max_{j\in\mathcal{I}} \|e_j^{n-1}\|_{C(\partial\Omega_j)}, \tag{23}$$

where $\mathcal{I} := \{1, \dots, N\}$ *and* $0 < \rho < 1$. *The convergence factor* ρ *is given by*

$$\rho = \max_{j\in\mathcal{I}} \max_{\ell\in\mathcal{I}_j} \max_{\overline{\Omega}_j\cap\partial\Omega_\ell} w_j, \tag{24}$$

where w_j *is the solution to*

$$\begin{aligned} -\Delta w_j &= 0 \quad \textit{in } \Omega_j, \\ w_j &= 1 \quad \textit{on } \partial\Omega_j \setminus \Gamma_{j,0}, \\ w_j &= 0 \quad \textit{on } \Gamma_{j,0}, \end{aligned} \tag{25}$$

and $\Gamma_{j,0} := \partial\Omega_j \setminus \bigcup_{k\in\mathcal{I}_j}(\Omega_k \cap \partial\Omega_j)$ *(as in* (2)*). Moreover, it holds that*

$$\max_{j\in\mathcal{I}} \|e_j^n\|_{C(\overline{\Omega}_j)} \le \rho^n \max_{j\in\mathcal{I}} \|e_j^0\|_{C(\overline{\Omega}_j)}. \tag{26}$$

Proof. Consider the jth subdomain. The corresponding solution to (6) is obtained by the Poisson kernel (7):

$$e_j^n(r,\varphi) = \int_{-\pi}^{\pi} P_r(\varphi - t) g_j^n(t) dt. \tag{27}$$

Recall g_j^n defined in (5):

$$g_j^n = \begin{cases} 0 & \text{on } \Gamma_{j,0}, \\ e_k^{n-1} & \text{on } \partial\Omega_j \cap \overline{\Omega}_k. \end{cases} \tag{28}$$

As discussed in section 2, the condition $e_j^0 \in C(\overline{\Omega}_j)$, for $j \in \mathcal{I}$, guarantees that $e_j^n \in C^2(\Omega_j) \cap C(\overline{\Omega}_j)$ for any n. Using (27) and (28) and recalling that (1a) holds, the solution $e_j^n(r,\varphi)$ can be bounded by

$$\begin{aligned} |e_j^n(r,\varphi)| &= \left| \int_{-\pi}^{\pi} P_r(\varphi - t) g_j^n(t) dt \right| = \left| \sum_{\ell\in\mathcal{I}_j} \int_{\partial\Omega_j\cap\overline{\Omega}_\ell} P_r(\varphi - t) e_\ell^{n-1}(t) dt \right| \\ &\le \sum_{\ell\in\mathcal{I}_j} \int_{\partial\Omega_j\cap\overline{\Omega}_\ell} P_r(\varphi - t) |e_\ell^{n-1}(t)| dt \\ &\le \sum_{\ell\in\mathcal{I}_j} \max_{\partial\Omega_j\cap\overline{\Omega}_\ell} |e_\ell^{n-1}| \int_{\partial\Omega_j\cap\overline{\Omega}_\ell} P_r(\varphi - t) dt \\ &\le \left[\max_{\ell\in\mathcal{I}_j} \max_{\partial\Omega_j\cap\overline{\Omega}_\ell} |e_\ell^{n-1}| \right] w_j(r,\varphi), \end{aligned} \tag{29}$$

where we used the triangle inequality, and the fact that the Poisson kernel $P_r(\varphi - t)$ is nonnegative, and we notice that the integral

$$\sum_{\ell\in\mathcal{I}_j} \int_{\partial\Omega_j\cap\overline{\Omega}_\ell} P_r(\varphi - t) dt = \int_{\partial\Omega_j\setminus\Gamma_{j,0}} P_r(\varphi - t) dt$$

is the solution $w_j(r,\varphi)$ to problem (25). The estimate (29) implies that

$$\max_{\ell\in\mathcal{I}_j} \max_{\overline{\Omega}_j\cap\partial\Omega_\ell} |e_j^n| \le \max_{\ell\in\mathcal{I}_j} \max_{\partial\Omega_j\cap\overline{\Omega}_\ell} |e_\ell^{n-1}| \max_{\ell\in\mathcal{I}_j} \max_{\overline{\Omega}_j\cap\partial\Omega_\ell} w_j, \tag{30}$$

and therefore for any $j \in \mathcal{I}$ we get

$$\begin{aligned} \max_{\ell\in\mathcal{I}_j}\max_{\overline{\Omega}_j\cap\partial\Omega_\ell}|e_j^n| &\le \max_{\ell\in\mathcal{I}_j}\max_{\partial\Omega_j\cap\overline{\Omega}_\ell}|e_\ell^{n-1}|\max_{k\in\mathcal{I}}\max_{\ell\in\mathcal{I}_k}\max_{\overline{\Omega}_k\cap\partial\Omega_\ell} w_k \\ &= \rho\max_{\ell\in\mathcal{I}_j}\max_{\partial\Omega_j\cap\overline{\Omega}_\ell}|e_\ell^{n-1}|, \end{aligned} \tag{31}$$

where we used (24). Now, (31) allows us to write

$$\max_{j\in\mathcal{I}}\max_{\ell\in\mathcal{I}_j}\max_{\overline{\Omega}_j\cap\partial\Omega_\ell}|e_j^n| \le \rho\max_{j\in\mathcal{I}}\max_{\ell\in\mathcal{I}_j}\max_{\partial\Omega_j\cap\overline{\Omega}_\ell}|e_\ell^{n-1}|. \tag{32}$$

Now, notice that the left-hand side is a maximum estimate of the data provided to step $n+1$ of the method, i.e.,

$$\max_{j\in\mathcal{I}}\max_{\ell\in\mathcal{I}_j}\max_{\overline{\Omega}_j\cap\partial\Omega_\ell}|e_j^n| = \max_{j\in\mathcal{I}}\|e_j^{n+1}\|_{C(\partial\Omega_j)},$$

while the term in the right-hand side is a maximum estimate of the data provided to step n of the method, i.e.,

$$\max_{j\in\mathcal{I}}\max_{\ell\in\mathcal{I}_j}\max_{\partial\Omega_j\cap\overline{\Omega}_\ell}|e_\ell^{n-1}| = \max_{j\in\mathcal{I}}\|e_j^{n}\|_{C(\partial\Omega_j)}.$$

Therefore, the estimate (32) implies that

$$\max_{j\in\mathcal{I}}\|e_j^{n+1}\|_{C(\partial\Omega_j)} \le \rho\max_{j\in\mathcal{I}}\|e_j^{n}\|_{C(\partial\Omega_j)}, \tag{33}$$

which is (23) with (24). The fact that $0<\rho<1$ follows by the maximum principle applied to the solution of (25).

Next, we recall that $e_j^n \in C^2(\Omega_j)\cap C(\overline{\Omega}_j)$ and we can invoke the weak maximum principle to write that $\|e_j^n\|_{C(\partial\Omega_j)} = \|e_j^n\|_{C(\overline{\Omega}_j)}$; see, e.g., [9, section 6.4.1, Theorem 1]. A simple recursion argument then leads to (26). ∎

We remark that Theorem 7, under the assumption (1), ensures that the PSM for the solution of linear, ringed, branched, and meshed chains converges geometrically in the continuous norm. In order to study the convergence behavior with respect to the number of subdomains, a more detailed discussion of the convergence factor ρ given in (24) is required. The convergence factor ρ is related to the solutions w_j of (25) and the geometry of the chain. Consider, for example, an equidistant linear chain $\mathcal{C}$ of N collinear subdomains, that is, the centers of the subdomains Ω_j are collinear. In this case, because of the regular geometry of the chain and recalling that according to Definition 2 the subdomains have the same radius equal to 1, it holds that $w_j = w_k$ for any $j,k = 2,\dots,N-1$. Notice also that $w_1 \le w_j$ and $w_N \le w_j$ for $j = 1,\dots,N$. Therefore, the convergence factor ρ does not depend on the number of subdomains. This result is summarized in Corollary 8.

COROLLARY 8. *Consider an equidistant linear chain $\mathcal{C}$ of N subdomains (unit disks according to Definition 2) such that the center of the subdomains Ω_j are collinear and $N > 2$.*[2] *Consider another subdomain Ω_{N+1} (a unit disk) whose center is collinear with the ones of Ω_j and such that the chain $\mathcal{C}' := \mathcal{C}\cup\Omega_{N+1}$ is still equidistant. Denote by $\mathcal{I}' := \mathcal{I}\cup\{N+1\}$; then the PSM converges geometrically in the sense that*

$$\max_{j\in\mathcal{I}'}\|e_j^n\|_{C(\overline{\Omega}_j)} \le \rho^n\max_{j\in\mathcal{I}'}\|e_j^0\|_{C(\overline{\Omega}_j)},$$

where ρ is exactly the convergence factor corresponding to the chain $\mathcal{C}$ given by (24).

[2]For $N=2$ the estimate is sharper and the convergence factor is given by $\rho = 1-\frac{2\alpha}{\pi}$ according to (19) with $\widetilde{\alpha} = \pi-\alpha$.

The previous result can be generalized to any equidistant linear chain and a precise estimate of the convergence factor ρ can be obtained by means of the results obtained in section 3. To do so, we notice that in the case that Ω_j are (unit) disks, the hypothesis (1) can be reformulated as follows: let Ω_j, Ω_k, and Ω_ℓ be any three atoms belonging to a chain $\mathcal{C}$ such that $\Omega_j \cap \Omega_k \neq \emptyset$ and $\Omega_k \cap \Omega_\ell \neq \emptyset$; then the two segments connecting the center of Ω_k with the centers of Ω_j and Ω_ℓ form an angle γ_k such that $2\cos\alpha\sin(\gamma_k/2) > 1$ (see Figure 10). We can now define the minimal angle γ as follows.

DEFINITION 9. *Consider an equidistant chain $\mathcal{C}$ and denote by γ_k the angles between the subdomains. The chain $\mathcal{C}$ is said to possess a minimal angle if there exists a constant $\epsilon > 0$ and an angle γ such that $2\cos\alpha\sin(\gamma/2) = 1+\epsilon$ and $\gamma < \min_k \gamma_k$. The angle γ is called the minimal angle.*

If a chain possesses a minimal angle, then (1) is satisfied. Once the angle γ is introduced, we can prove our next convergence result. To do so, we need the following lemma.

LEMMA 10. *Consider the two triangles $\overline{P_1CO_2}$ and $\overline{O_1CO_2}$ in Figure 11. Assume that $|Q-C| = |P_1-C|$ and that the two circles have unitary radius, that is, $|P_1-O_2| = |Q| = 1$. Then we have*

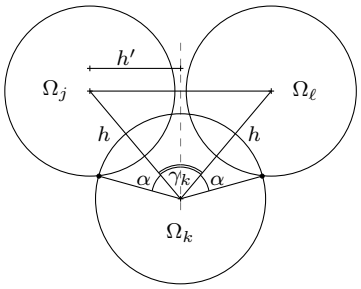

FIG. 10. *Details of three subdomains satisfying* (1). *Notice that $h = 2\cos\alpha$ and since Ω_j, Ω_k, and Ω_ℓ are unit disks, the condition $h' = h\sin(\gamma/2) > 1$ ensures that $\Omega_j \cap \Omega_\ell = \emptyset$.*

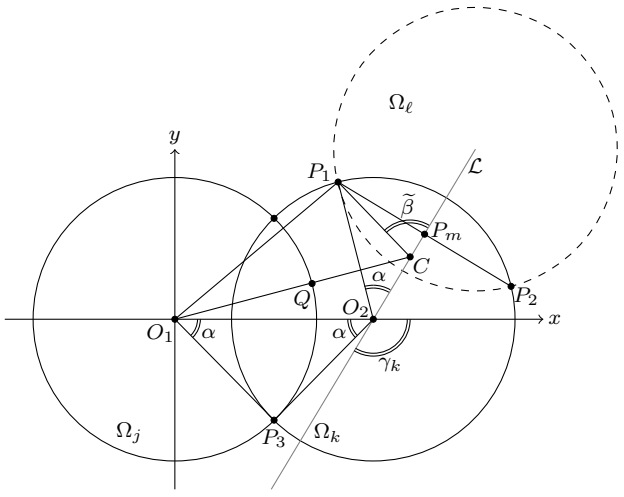

FIG. 11. *Details of the geometry considered in the proof of Theorem* 11.

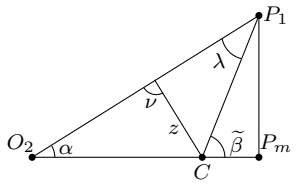

FIG. 12. *Details of the two triangles* $\overline{P_1O_2C}$ *and* $\overline{P_1O_2P_m}$ *extracted from Figure* 11. *Notice that* z *denotes the height of* $\overline{P_1O_2C}$ *and* $\nu = \pi/2$.

$$|C - O_2|^2 - 2|C - O_2|\cos\alpha = |C|^2 - 2|C| \tag{34}$$

and

$$|C|^2 = |C - O_2|^2 + 4(\cos\alpha)^2 - 4|C - O_2|\cos\gamma_k\cos\alpha. \tag{35}$$

Proof. Since the vectors C and Q are collinear, we have that

$$|C| = |Q| + |C - Q|.$$

Combining this with the assumptions $|Q - C| = |P_1 - C|$ and $|Q| = 1$, we obtain

$$|P_1 - C| = |C| - 1. \tag{36}$$

Consider the triangle $\overline{P_1CO_2}$ shown in Figure 12. The length of its sides are $|P_1 - C|$, $|C - O_2|$, and $|P_1 - O_2|$. The height z of the triangle is $|C - O_2|\sin\alpha$, and the projection of $\overline{CO_2}$ on $\overline{P_1O_2}$ has length $|C - O_2|\cos\alpha$. Hence, the Pythagoras theorem allows us to write

$$(|P_1 - O_2| - |C - O_2|\cos\alpha)^2 + |C - O_2|^2(\sin\alpha)^2 = |P_1 - C|^2.$$

Recalling (36) and that $|P_1 - O_2| = 1$, the previous relation gives (34).

Now, consider the triangle $\overline{O_1CO_2}$. The length of its sides are $|C|$, $|C - O_2|$, and $|O_1 - O_2|$. Notice that $|O_1 - O_2| = 2\cos\alpha$. The height of the triangle is $|C - O_2|\sin\gamma_k$, and the projection of $\overline{CO_2}$ on $\overline{O_1O_2}$ has length $|C - O_2|\cos\gamma_k$. Again the Pythagoras theorem gives us

$$(2\cos\alpha - |C - O_2|\cos\gamma_k)^2 + |C - O_2|^2(\sin\gamma_k)^2 = |C|^2,$$

and this yields (35). ∎

We are ready to prove the next convergence result. Notice that in Theorem 11 we assume that $\alpha \in (0, \pi/3)$. This is because for $\alpha \geq \pi/3$ three consecutive atoms Ω_j, Ω_k, and Ω_ℓ have nonempty intersection, that is, $\overline{\Omega}_j \cap \overline{\Omega}_k \cap \overline{\Omega}_\ell \neq \emptyset$, which contradicts our assumption (1).

THEOREM 11. *Consider an equidistant linear chain* $\mathcal{C}$ *of* N *subdomains (unit disks according to Definition* 2*) that possesses a minimal angle* γ *and such that* $\alpha \in (0, \pi/3)$. *Then the PSM* (6) *converges geometrically in the sense that*

$$\max_{j\in\mathcal{I}} \|e_j^n\|_{C(\overline{\Omega}_j)} \leq \rho(\alpha,\gamma)^n \max_{j\in\mathcal{I}} \|e_j^0\|_{C(\overline{\Omega}_j)},$$

where the convergence factor $\rho(\alpha, \gamma)$ *depends on the angles* α *and* γ *(as in Figure* 10*) and is given by*

$$\rho(\alpha,\gamma) = 1 - \frac{3\alpha - \widetilde{\beta}(\alpha,\gamma)}{\pi}, \tag{37}$$

where

$$\widetilde{\beta}(\alpha,\gamma) = \arcsin\left(\frac{f_1(\alpha,\gamma)}{f_2(\alpha,\gamma)-1}\sin\alpha\right) + \alpha \tag{38}$$

with

$$\begin{aligned} f_1(\alpha,\gamma) = & \frac{-2\cos\alpha\left[\left(f_3(\alpha,\gamma)\right)^2+\cos\gamma\right]}{\left(f_3(\alpha,\gamma)\right)^2-1} \\ & + \frac{2\cos\alpha\sqrt{\left[\left(f_3(\alpha,\gamma)\right)^2+\cos\gamma\right]^2-\left[\left(f_3(\alpha,\gamma)\right)^2-1\right]\left((\cos\alpha)^2-1\right)}}{\left(f_3(\alpha,\gamma)\right)^2-1} \end{aligned} \tag{39}$$

and

$$f_2(\alpha,\gamma) = f_1(\alpha,\gamma)f_3(\alpha,\gamma) + 2(\cos\alpha)^2, \quad f_3(\alpha,\gamma) = \left[1-2\cos\gamma\right]\cos\alpha. \tag{40}$$

Consider another subdomain Ω_{N+1} (unit disk) such that the chain $\mathcal{C}' := \mathcal{C}\cup\Omega_{N+1}$ is linear and equidistant and has the same minimal angle γ of $\mathcal{C}$. Denote by $\mathcal{I}' := \mathcal{I}\cup\{N+1\}$; then the PSM converges geometrically in the sense that

$$\max_{j\in\mathcal{I}'}\|e_j^n\|_{C(\overline{\Omega}_j)} \le \rho^n \max_{j\in\mathcal{I}'}\|e_j^0\|_{C(\overline{\Omega}_j)}, \tag{41}$$

where ρ is exactly the convergence factor corresponding to the chain $\mathcal{C}$ given by (37).

Proof. The geometric convergence follows from Theorem 7. We are now interested in the estimate of ρ given by (24). Hence we need to study the solution w_j to problem (25). To do so, we consider the geometric setting given in Figure 11, where the intersection of Ω_j, Ω_k, and Ω_ℓ and the angle γ_k are represented.

Since the chain $\mathcal{C}$ considered is linear, each of the w_j's solves the problem (25) that is similar to problem (21) analyzed in Theorem 6 (see also Figure 9). Therefore, according to Theorem 6 the solution w_k along the arc given by $\overline{\partial\Omega_j\cap\Omega_k}$, that has extrema in P_3 and P_4, admits a unique maximum in a point Q (Figure 11) and assumes the value given by (22). Since Ω_j, Ω_k, and Ω_ℓ are unit disks and equidistant, we have that $\beta=\alpha$ and $\widetilde{\alpha}=\pi-\alpha$ and (22) becomes

$$w_k(Q) = 1 - \frac{3\alpha-\widetilde{\beta}}{\pi}.$$

Now, we need to determine $\widetilde{\beta}$ which is related to the position of Q on $\overline{\partial\Omega_j\cap\Omega_k}$. To do so, we recall that we are looking for a circle passing trough the points P_1 and P_2 and tangent to the arc $\overline{\partial\Omega_j\cap\Omega_k}$ at the point Q. The center C of this circle lies on the straight line $\mathcal{L}$ that bisects the segment $\overline{P_1P_2}$ and passes through the center O_2 of Ω_k. Since the points Q and P_1 lie on this circle, we have that $|Q-C| = |P_1-C|$. Therefore, the assumptions of Lemma 10 are satisfied and it holds that

$$\begin{aligned} |C|^2 - 2|C| &= |C-O_2|^2 - 2|C-O_2|\cos\alpha, \\ |C|^2 &= |C-O_2|^2 + 4(\cos\alpha)^2 - 4|C-O_2|\cos\gamma_k\cos\alpha, \end{aligned} \tag{42}$$

which is a system of two equations where the two unknowns are $|C|$ and $|C-O_2|$. A straightforward calculation shows that the admissible solution to (42) is

$|C - O_2| = f_1(\alpha, \gamma_k)$ and $|C| = f_2(\alpha, \gamma_k)$, where $f_1(\alpha, \gamma_k)$ and $f_2(\alpha, \gamma_k)$ are given by (39) and (40). Next, consider the two triangles $\overline{P_1 O_2 C}$ and $\overline{P_1 O_2 P_m}$; see Figure 12. Notice that $\widetilde{\beta} = \lambda + \alpha$ and that the height z of $\overline{P_1 O_2 C}$ is

$$|C - O_2| \sin\alpha = z = |P_1 - C| \sin\lambda.$$

Therefore, recalling that $|P_1 - C| = |C| - 1$, we obtain

$$\widetilde{\beta}(\alpha, \gamma_k) = \arcsin\left(\frac{|C - O_2|}{|C| - 1} \sin\alpha\right) + \alpha, \tag{43}$$

which is equal to (38) up to the fact that γ_k appears in (43), while the minimal angle γ appears in (38). So far we have established that

$$\max_{\overline{\Omega}_k \cap \partial\Omega_j} w_k = 1 - \frac{3\alpha - \widetilde{\beta}(\alpha, \gamma_k)}{\pi}.$$

To complete the proof, we need to show that the map $[\gamma, \pi] \ni \xi \mapsto 1 - \frac{3\alpha - \widetilde{\beta}(\alpha,\xi)}{\pi}$ is monotonically decreasing in ξ for $\alpha \in [0, \pi/3]$. Since the arcsin is strictly monotonically increasing, it is sufficient to show that the map $[\gamma, \pi] \ni \xi \mapsto F_\alpha(\xi) := \frac{f_1(\alpha,\xi)}{f_2(\alpha,\xi)-1}$ is strictly monotonically decreasing. To do so, we define $g(\alpha) := 2(\cos\alpha)^2 - 1$, and we notice that $F_\alpha(\xi)$ has the form

$$F_\alpha(\xi) = \frac{f_1(\alpha, \xi)}{f_1(\alpha, \xi) f_3(\alpha, \xi) + g(\alpha)}.$$

Differentiating this with respect to ξ allows us to obtain

$$F'_\alpha(\xi) = \frac{f'_1(\alpha, \xi) g(\alpha) - (f_1(\alpha, \xi))^2 f'_3(\alpha, \xi)}{(f_1(\alpha, \xi) f_3(\alpha, \xi) + g(\alpha))^2},$$

where the superscript $'$ denotes the derivative with respect to ξ. A direct calculation shows that $f'_3(\alpha, \xi) = 2 \sin\xi \cos\alpha \geq 0$ and $g(\alpha) \geq 0$ for $\xi \in [\gamma, \pi]$ and $\alpha \in [0, \pi/3]$. Therefore, to obtain that F_α is monotonically decreasing, it is sufficient to show that $f'_1(\alpha, \xi) \leq 0$, which can be achieved by a direct calculation. ∎

5. Examples and numerical experiments. In this section, we use the results obtained in sections 3 and 4 to study the convergence behavior of the PSM. In particular, we study a linear chain of collinear atoms in section 5.1 and a ringed chain whose atoms have the centers distributed on a circle in section 5.2. In section 5.3, we discuss the convergence of the PSM for branched and meshed chains. In what follows, we assume that "to add another atom to a chain" means that a new atom is included in the chain without changing its structure, i.e., a linear chain remains linear, a ringed chain remains ringed, and a branched chain remains branched.

In each of the following sections, we present results of numerical experiments and compare them with our theoretical results. In particular, we have performed numerical simulations based on a P1-finite-elements discretization of the subdomain problems. To compare the results of such numerical simulations with our theoretical estimates, we recall that the contraction factor satisfies

$$\frac{\max_{j \in \mathcal{I}} \|e_j^n\|_{C(\overline{\Omega}_j)}}{\max_{j \in \mathcal{I}} \|e_j^0\|_{C(\overline{\Omega}_j)}} \leq \rho(\alpha)^n.$$

In the case, if we stop the iterations when $\frac{\max_{j \in \mathcal{I}} \|e_j^n\|_{C(\overline{\Omega}_j)}}{\max_{j \in \mathcal{I}} \|e_j^0\|_{C(\overline{\Omega}_j)}} \leq \texttt{Tol}$, where `Tol` is a given tolerance, we obtain

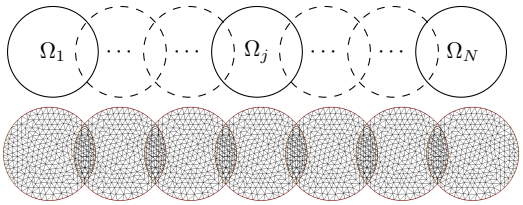

FIG. 13. *Example of a linear chain with minimal angle $\gamma = \pi$ (top) and example of corresponding finite-element discretization (bottom).*

$$\texttt{Tol} \approx \frac{\max_{j\in\mathcal{I}} \|e_j^n\|_{C(\overline{\Omega}_j)}}{\max_{j\in\mathcal{I}} \|e_j^0\|_{C(\overline{\Omega}_j)}} \leq \rho(\alpha)^n,$$

which allows us to get the estimate

$$n \leq \frac{|\log(\texttt{Tol})|}{|\log(\rho(\alpha))|}. \tag{44}$$

In all our numerical experiments we set $\texttt{Tol} = 10^{-6}$ and calculate an upper bound for the number of iterations n using (44). We can therefore compare this upper bound with the number of iterations performed by our numerical realizations.

5.1. Linear chains. Consider a linear chain of collinear atoms such that the domain Ω_j of the jth atom is a unit ball in $\mathbb{R}^2$ and intersects both Ω_{j-1} and Ω_{j+1} as depicted in Figure 13. Since all the centers of the atoms are collinear the minimal angle is $\gamma = \pi$. Notice that this case is a two-dimensional version of the chain problem presented in [5, Figure 10]. Theorem 11 ensures that the PSM converges independently of N in the sense that

$$\max_{j\in\mathcal{I}} \|e_j^n\|_{C(\overline{\Omega}_j)} \leq \rho(\alpha)^n \max_{j\in\mathcal{I}} \|e_j^0\|_{C(\overline{\Omega}_j)},$$

where the convergence factor $\rho(\alpha)$ does not depend on N:

$$\rho(\alpha) = 1 - \frac{2\alpha}{\pi} + \frac{1}{\pi} \arcsin\left(\frac{f_1(\alpha,\pi)}{f_2(\alpha,\pi) - 1} \sin\alpha\right).$$

Here f_1 and f_2 are given in (39) and (40), and we used the fact that $\gamma = \pi$. The map $\alpha \mapsto \rho(\alpha)$ is shown in Figure 14 (left). The range of α is $[0, \pi/3]$, since for $\alpha \geq \pi/3$ one has $\overline{\Omega}_j \cap \overline{\Omega}_k \cap \overline{\Omega}_\ell \neq \emptyset$, contradicting hypothesis (1). Notice that $\rho(\alpha) = 1$ for $\alpha = 0$ (no overlap),[3] $\rho(\alpha) < 1$ for $\alpha > 0$, and $\rho(\alpha)$ decreases for α increasing in the range $(0, \widetilde{\alpha})$ with $\widetilde{\alpha} \approx 0.8411$. Since α represents (in some sense) the overlap, this behavior is in agreement with the convergence factors of the classical PSM presented in the literature for other applications; see, e.g., [10, Figure 4.1] and [6, Figure 4]. However, $\rho(\alpha)$ attains a minimum at $\widetilde{\alpha}$ and increases for $\alpha > \widetilde{\alpha}$. This is a very unusual behavior for classical PSM and is in contrast to classical Schwarz theory for Laplace like problems. To explain it we use Figure 14 (right), where the value $|P_1 - C|$ (see Figure 11) is shown as a function of α. Comparing Figures 11 and 9, we see that

[3] If there is no overlap, however, the method converges in one iteration, since the subdomains are decoupled, so there is a discontinuity in the convergence factor.

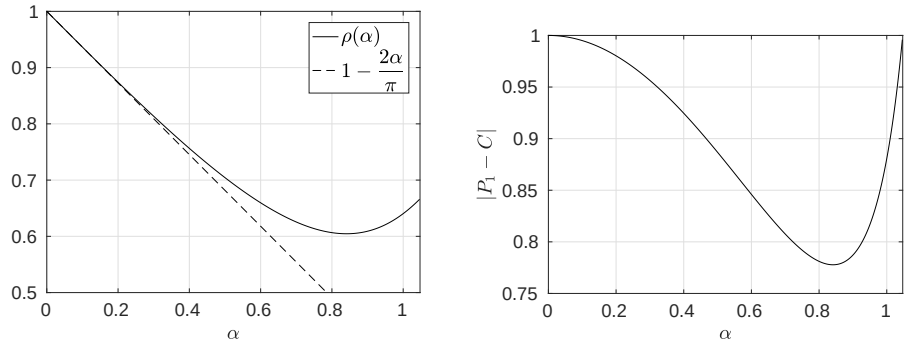

FIG. 14. *Left: the convergence factor $\rho(\alpha)$ of the PSM for the solution of a linear chain of N collinear atoms. This factor is compared with the linear function $1-\frac{2\alpha}{\pi}$ that is the convergence factor of a chain of two atoms. Right: values of $|P_1-C|$ with respect to the angle α. Notice that both $\rho(\alpha)$ and $|P_1-C|$ attain a minimum at $\alpha=\widetilde{\alpha}\approx 0.8411$.*

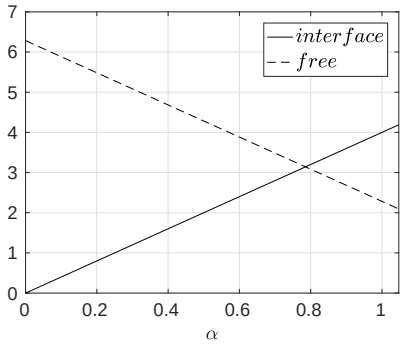

FIG. 15. *Length of interface (solid line) and free boundary (dashed line) for an internal atom Ω_j of the equidistant linear chain of collinear atoms depicted in Figure* 13.

$|P_1-C|$ is the radius of the arc $\mathcal{A}^r_{\widetilde{\beta}}$ that produces the maximum on the interface $\mathcal{A}^\ell_{\widetilde{\alpha}}$. The radius $|P_1-C|$ attains also its minimum at $\widetilde{\alpha}$, which means that the combination of the effects of the two interfaces gives the minimal contribution to $\rho(\alpha)$. A heuristic explanation of the nonlinear behavior of $\rho(\alpha)$ can be given by evaluating the length of the interface and the free boundary as a function of α for an atom Ω_j in the linear chain. In particular, since Ω_j is a unit disc, the length of the interface characterized by α is 2α (this is the length of the arc corresponding to the angle 2α). Since there are two interfaces for Ω_j, the total length is 4α. This is depicted in Figure 15 (solid line). The free boundary length is then $2\pi-4\alpha$ (dashed line in Figure 15). We see in Figure 15 that the contribution of the free boundary dominates until $\alpha\approx 0.8$, which is very close to $\widetilde{\alpha}$. For $\alpha>0.8$, the contribution of the free boundary is dominated and this indicates a loss of convergence speed corresponding to the increase in the convergence factor $\rho(\alpha)$ for $\alpha>\widetilde{\alpha}$. Furthermore, in Figure 14 (left) the convergence factor $\rho(\alpha)$ is compared with the linear function $1-\frac{2\alpha}{\pi}$ that is the convergence factor for a chain of only two atoms. We see that for α small the convergence factor of a linear chain of N atoms has a very similar behavior to the convergence factor of the 2-atom chain. For larger α, however, the two are very different. The unexpected growth of $\rho(\alpha)$ for $\alpha>\widetilde{\alpha}$ was absent when studying the PSM for a linear chain

TABLE 1
Number of iterations performed by the PSM for the solution of linear chains of collinear subdomains within a tolerance of 10^{-6}. *The bound estimated as* $\frac{|\log(Tol)|}{|\log(\rho(\alpha))|}$ *is indicated in parentheses.*

N	$\alpha = 0.2$	$\alpha = 0.4$	$\alpha = 0.6$	$\alpha = 0.8$	$\alpha = 1.0$
2	80 (99)	41 (50)	25 (33)	18 (27)	13 (30)
4	81 (99)	41 (50)	27 (33)	20 (27)	17 (30)
6	81 (99)	42 (50)	27 (33)	21 (27)	18 (30)
8	81 (99)	42 (50)	27 (33)	21 (27)	18 (30)
10	81 (99)	42 (50)	27 (33)	21 (27)	18 (30)
20	81 (99)	42 (50)	27 (33)	21 (27)	18 (30)
30	81 (99)	42 (50)	27 (33)	21 (27)	18 (30)
40	81 (99)	42 (50)	27 (33)	21 (27)	18 (30)
50	81 (99)	42 (50)	27 (33)	21 (27)	18 (30)

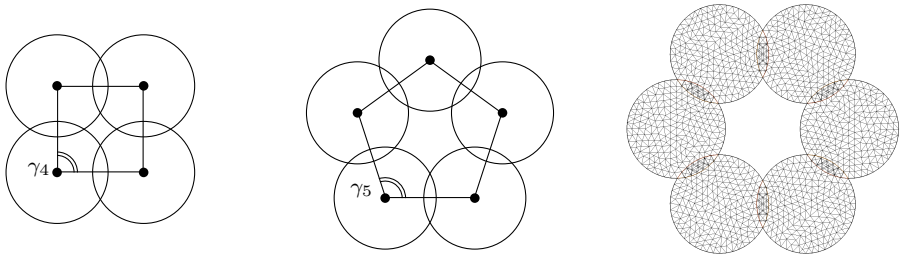

FIG. 16. *Ringed chains of* $N = 4, 5, 6$ *atoms and their minimal angles* $\gamma_4 = \pi/2$ *and* $\gamma_5 = 3\pi/5$. *The right figure is an example of a finite-element discretization of a ringed chain of* $N = 6$ *subdomains centered at the verteces of a hexagon.*

with approximate rectangular geometry (see [6, Figure 4]) and shows that for the understanding of molecular simulations with PSM, using the correct geometry in the analysis is important.

In Table 1 we show the number of iterations performed by our numerical experiments. An example of a finite-element discretization is given in Figure 13. It is clear that the number of performed iterations does not decay linearly with respect to α (the overlap) but follows a nonlinear pattern as indicated by our estimate of the contraction factor $\rho(\alpha)$. Notice how the numbers of performed iterations corresponding to $\alpha = 0.8$ (21) and $\alpha = 1.0$ (18) are very similar.

5.2. Ringed chains. In this section, we present an example that resembles the test case considered in [5, Figure 11]. The example presented in [5] considers a sequence of ringed chains of equidistant subdomains (unit disks according to Definition 2) whose centers are distributed on a circle of fixed radius. Hence, for N sufficiently large, the assumption (1a) is violated. For this reason, we consider a sequence $\mathcal{C}_N$ of ringed equidistant chains where the distance between the centers of the subdomains is fixed. Assume that for each chain the centers of the elements in the chain are the vertices of a regular polygon and that the different polygons have sides of identical length. This means that the distance between the subdomains of $\mathcal{C}_N$ is equal to the distance between the subdomains of $\mathcal{C}_{N+1}$. An example of such chains is given in Figure 16, where $\mathcal{C}_4$, $\mathcal{C}_5$, and $\mathcal{C}_6$ are shown. We will see that, in contrast to the other chains discussed in this paper, the sequence of chains considered in this section is characterized by a convergence factor that decays as N increases. This is a further very unusual behavior for a one-level Schwarz method due to the specific geometry of the problem. The minimal angle of the chain $\mathcal{C}_N$ coincides with the internal angle of the corresponding regular polygon having N sides, namely,

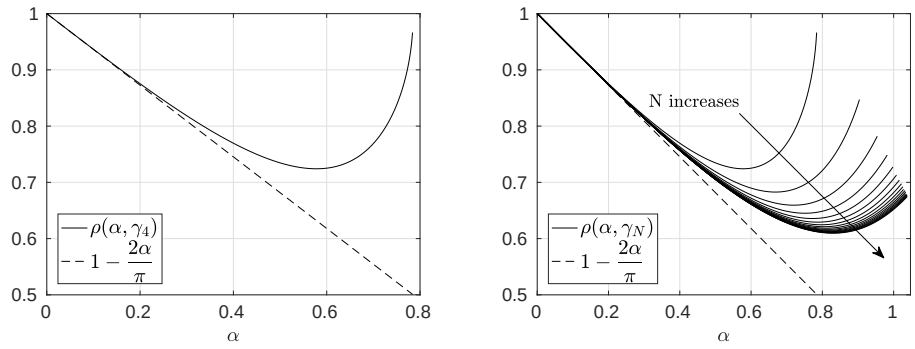

FIG. 17. *Left: convergence factor $\rho(\alpha,\gamma_4)$ of the PSM for the solution of an equidistant ringed chain of $N=4$ atoms. Right: convergence factors $\rho(\alpha,\gamma_N)$ of the PSM for the solution of equidistant ringed chains of N atoms.*

$$\gamma_N = \frac{\pi(N-2)}{N},$$

and it holds that $\gamma_N < \gamma_{N+1}$. Therefore, Theorem 11 ensures that the PSM for the solution of $\mathcal{C}_N$ converges geometrically with a convergence factor $\rho(\alpha,\gamma_N)$. Moreover, since the map $\gamma \mapsto \rho(\alpha,\gamma)$ is monotonically decreasing we have

$$\rho(\alpha,\gamma_N) \le \rho(\alpha,\gamma_{N-1}) \le \cdots \le \rho(\alpha,\gamma_5) \le \rho(\alpha,\gamma_4).$$

This means that $\rho(\alpha,\gamma_N)$ is bounded by $\rho(\alpha,\gamma_4)$. Therefore, the convergence factor does not deteriorate when the number of atoms increases; it even improves. The factors $\rho(\alpha,\gamma_N)$ for $N=4,\dots,20$ are shown in Figure 17. We see that for a given α, the convergence factor decreases when N increases. The upper curve on the left of Figure 17 corresponds to $N=4$ and the last curve at the bottom corresponds to $N=20$. Each curve is computed for $\alpha \in [0,\widehat{\alpha}]$, where $\widehat{\alpha}$ satisfies the minimal angle condition $2\cos(\widehat{\alpha})\sin(\gamma_N/2)$. We see that when N increases, the convergence factor of the ringed chain converges to the convergence factor of the linear equidistant chain shown in Figure 14.

In Table 2 we show the number of iterations performed by our numerical experiments based on a finite-element discretization of the Schwarz subproblems; see, e.g., Figure 16 (right). The number of iterations performed does not decay linearly with respect to α (the overlap) but follows a nonlinear pattern as indicated by our estimate of the contraction factor $\rho(\alpha)$ given in Figure 17.

5.3. Branched and meshed chains. Consider a branched chain $\mathcal{C}$ obtained as the union of linear subchains $\mathcal{C}_\ell$, that is, $\mathcal{C} = \cup_\ell \mathcal{C}_\ell$ (recall Definition 1). The notion of minimal angle allows us to study linear and ringed chains, hence the subchains $\mathcal{C}_\ell$. Therefore, the analysis of each subchain can be performed similarly as in sections 5.1 and 5.2. The main difference between branched chains and linear/ringed chains is in the connection atoms that are the elements connecting different subchains. The cases of connection atoms is more subtle, because they are strongly affected by the geometry of the chain, and one should precisely define the meaning of "adding a new subdomain to the chain."

To study the convergence of a branched chain, denote by γ_ℓ and $\rho_\ell(\alpha) := \rho(\alpha,\gamma_\ell)$ the minimal angle and the convergence factor of the (linear/ringed) subchain $\mathcal{C}_\ell$. The convergence factor of the branched chain $\mathcal{C}$ can be estimated by

$$\rho(\alpha) = \max\Big\{\max_\ell \rho_\ell^c(\alpha),\, \max_\ell \rho_\ell(\alpha)\Big\},$$

TABLE 2
Number of iterations performed by the PSM for the solution of ringed chains of subdomains within a tolerance of 10^{-6}. *The bound estimated as* $\frac{|\log(Tol)|}{|\log(\rho(\alpha))|}$ *is indicated in parentheses.*

N	$\alpha = 0.1$	$\alpha = 0.3$	$\alpha = 0.5$	$\alpha = 0.7$
4	173 (190)	56 (79)	34 (38)	30 (32)
5	179 (190)	53 (79)	33 (38)	26 (32)
6	183 (190)	53 (79)	33 (38)	25 (32)
7	171 (190)	54 (79)	33 (38)	24 (32)
8	188 (190)	55 (79)	33 (38)	24 (32)
9	161 (190)	55 (79)	33 (38)	24 (32)
10	186 (190)	54 (79)	32 (38)	24 (32)
20	179 (190)	55 (79)	32 (38)	24 (32)
30	184 (190)	54 (79)	32 (38)	24 (32)
40	186 (190)	54 (79)	32 (38)	24 (32)
50	184 (190)	52 (79)	32 (38)	24 (32)

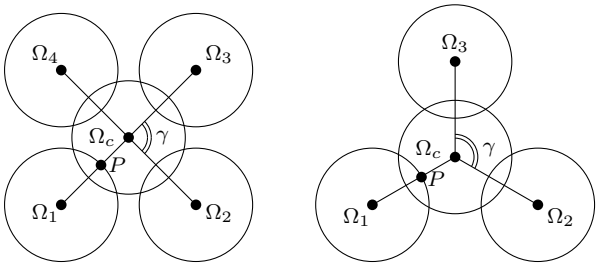

FIG. 18. *Left: connection atom* Ω_c *that intersects with four atoms with an angle* $\gamma = \pi/2$. *Right: connection atom* Ω_c *that intersects with three atoms with an angle* $\gamma = 2\pi/3$.

where $\rho_\ell^c(\alpha)$ is the convergence factor of the ℓth connection atom. If the addition of another atom to the chain $\mathcal{C}$ does not affect $\rho(\alpha)$, then the convergence is independent of the number of subdomains. This means that $\max_\ell \rho_\ell^c(\alpha)$ and $\max_\ell \rho_\ell(\alpha)$ are bounded by two quantities that are independent of the number of subdomains.

In what follows, we show how to use the results developed in sections 3 and 4 to estimate the convergence factors of connection atoms. In particular, we consider the two cases depicted in Figure 18. The first case (Figure 18, left) corresponds to a connection atom Ω_c that intersects with four atoms $\Omega_1, \ldots, \Omega_4$ distributed with an angle $\gamma = \pi/2$. To find the convergence factor, we need to study a problem similar to (21),

$$
\begin{aligned}
-\Delta w &= 0 \ \text{ in } \Omega_c, \\
w &= 1 \ \text{ on } \Gamma_1, \Gamma_2, \Gamma_3, \text{ and } \Gamma_4, \\
w &= 0 \ \text{ on } \partial\Omega_c \setminus \left(\bigcup_{\ell=1}^{4} \Gamma_\ell \right),
\end{aligned}
\tag{45}
$$

where $\Gamma_\ell := \partial\Omega_c \cap \overline{\Omega}_\ell$. Then the convergence factor is the maximum of w along $\overline{\Omega}_c \cap \partial\Omega_\ell$ for all ℓ. We observed by a direct calculation that, because of the symmetry in the geometry of problem (45), the maximum is attained at the midpoint of the arc $\overline{\Omega}_c \cap \partial\Omega_\ell$, which we denote by P (see Figure 18, left). The linearity of (45) allows us to decompose the solution w as $w = w_{1,3} + w_2 + w_4$, where $w_{1,3}$, w_2, and w_4 solve

$$
-\Delta w_{1,3} = 0 \ \text{ in } \Omega_c, \ w_{1,3} = 1 \ \text{ on } \Gamma_1 \text{ and } \Gamma_3, \ w_{1,3} = 0 \ \text{ on } \partial\Omega_c \setminus (\Gamma_1 \cap \Gamma_3),
$$

and

$$-\Delta w_\ell = 0 \text{ in } \Omega_c,\ w_\ell = 1 \text{ on } \Gamma_\ell,\ w_\ell = 0 \text{ on } \partial\Omega_c \setminus \Gamma_\ell,$$

for $\ell = 2, 4$. The symmetry of these problems allows us to write $w(P) = w_{1,3}(P) + 2w_2(P)$, since $w_2(P) = w_4(P)$. Theorem 11 can be used as in section 5.1 to obtain

$$w_{1,3}(P) = 1 - \frac{2\alpha}{\pi} + \frac{1}{\pi}\arcsin\left(\frac{f_1(\alpha,\pi)}{f_2(\alpha,\pi)-1}\sin\alpha\right).$$

Theorem 5 together with a cumbersome calculation based on geometric arguments allows us to compute

$$w_2(P) = \frac{1}{\pi}\arcsin\left(\frac{\sin\alpha}{\sqrt{8(\cos\alpha)^2 - 12\cos\alpha + 5}}\right) - \frac{\alpha}{\pi}.$$

Therefore, the convergence factor is

$$\begin{aligned}\rho(\alpha) = 1 &- \frac{2\alpha}{\pi} + \frac{1}{\pi}\arcsin\left(\frac{f_1(\alpha,\pi)}{f_2(\alpha,\pi)-1}\sin\alpha\right)\\ &+ \frac{2}{\pi}\arcsin\left(\frac{\sin\alpha}{\sqrt{8(\cos\alpha)^2 - 12\cos\alpha + 5}}\right) - \frac{2\alpha}{\pi}.\end{aligned} \tag{46}$$

The map $\alpha \mapsto \rho(\alpha)$ is shown in Figure 19 (left) for $\alpha \in [0, \pi/4]$. Notice that the convergence factor for $\alpha = \pi/4$ is $\rho(\pi/4) = 1$ as shown in Figure 19 (left). This is due to the fact that (1) is violated for $\alpha \geq \pi/4$. In fact, for $\alpha = \pi/4$ one has that $\bigcup_{\ell=1}^{4} \Gamma_\ell = \partial\Omega_c$, which means that $w = 1$ in $\overline{\Omega}_c$. This is thus a relevant example where our convergence analysis fails. It is shown in [5] by direct numerical experiments that the PSM converges even if (1) is violated. The results we obtained could be further refined in order to cover this and even more complicated geometries, which is, however, beyond the scope of the present paper.

The second case (Figure 18, right) corresponds to a connection atom Ω_c that intersects three atoms $\Omega_1, \Omega_2, \Omega_3$ distributed with an angle $\gamma = 2\pi/3$. Similar arguments as before allow us to estimate the convergence factor via the solution to

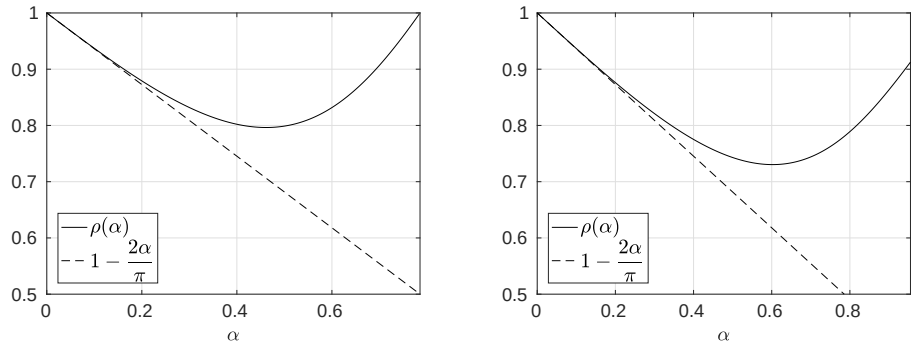

FIG. 19. *The figures on the left and the right, respectively, show the convergence factors $\rho(\alpha)$ corresponding to the connection atoms Ω_c depicted in Figure* 18*, left and right.*

$$\begin{aligned} -\Delta w &= 0 \ \text{ in } \Omega_c, \\ w &= 1 \ \text{ on } \Gamma_1, \Gamma_2, \ \text{and } \Gamma_3, \\ w &= 0 \ \text{ on } \partial\Omega_c \setminus \left(\bigcup_{\ell=1}^{3} \Gamma_\ell \right). \end{aligned}$$

The convergence factor is the maximum of w along $\overline{\Omega}_c \cap \partial\Omega_\ell$ for all ℓ. A direct calculation allows us to observe that, because of the symmetry in the geometry of problem (45), the maximum is attained at the point P (see Figure 18, right), and we have that $w(P) = w_1(P) + w_2(P) + w_3(P)$, where w_1, w_2, and w_3 solve

$$-\Delta w_\ell = 0 \ \text{ in } \Omega_c, \ w_\ell = 1 \ \text{ on } \Gamma_\ell, \ w_\ell = 0 \ \text{ on } \partial\Omega_c \setminus \Gamma_\ell,$$

for $\ell = 1, 2, 3$. Theorem 5 and a cumbersome calculation allows us to compute

$$\rho(\alpha) = 1 - \frac{4\alpha}{\pi} + \begin{cases} \frac{2}{\pi} \arcsin\big(z(\alpha)\big) & \text{if } z(\alpha) \le \pi/2, \\ \frac{2}{\pi} \arcsin\big(\pi - z(\alpha)\big) & \text{otherwise,} \end{cases} \tag{47}$$

where $z(\alpha) = \sin\alpha \left(\frac{6\cos(4\alpha) - 18\cos(3\alpha) + 44\cos(2\alpha) - 63\cos\alpha + 39}{8(\cos 2\alpha) - 8\cos\alpha + 9} \right)^{-1/2}$. The convergence factor $\rho(\alpha)$ is shown in Figure 19 (right).

Now the previous two examples can be used to determine the convergence factor of meshed chains. Consider the two examples of equidistant meshed chains depicted in Figures 20 and 21. Notice that these chains very much resemble crystal structures and therefore are not strictly related to a solvation model. Nonetheless, these configurations could be of wide interest in many domain-decomposition applications. The former is a chain whose subdomains have the centers distributed on a squared uniform grid, whereas the latter is composed by subdomains distributed on a grid with a "honeycomb" structure, which is reminiscent of the carbon structure. It is clear that the convergence factors corresponding to these chains are governed by the internal subdomains, which can be treated as for the cases depicted in Figure 18. Therefore, the convergence factors corresponding to the former and the latter meshed chains are given exactly by (46) and (47), respectively. Notice also that if we add to those chains other subdomains such that the geometric structure is preserved, then

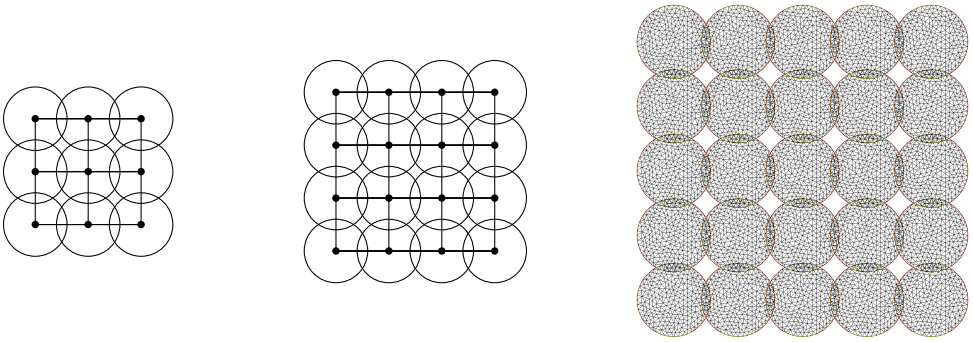

FIG. 20. *Meshed chains of $N = 9, 16, 25$ subdomains. Notice that each of the interior subdomains intersects with four neighbors and they can be treated as the example given in Figure* 18 *(left). Therefore, the convergence factor of these chains is $\rho(\alpha)$ given in* (46) *and depicted in Figure* 19 *(left). The right figure is an example of a finite-element discretization of a meshed chain of* 25 *subdomains.*

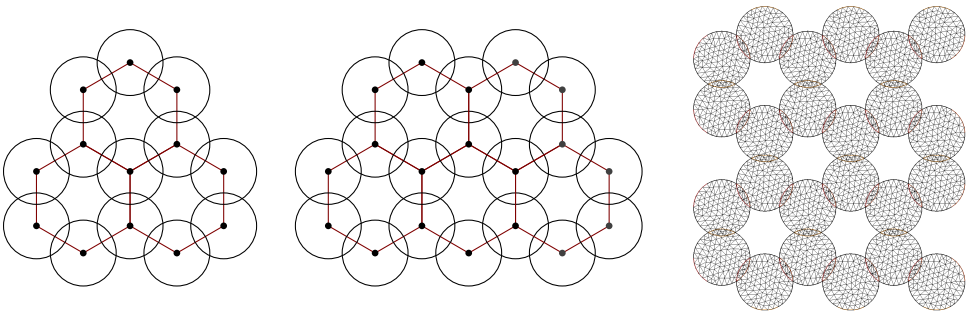

FIG. 21. *Meshed chains of $N = 13$, $N = 19$ and $N = 24$ subdomains. Notice that each of the internal subdomains intersect with four neighbors and they can be treated as the example given in Figure* 18 *(right). Therefore, the convergence factor of these chains is $\rho(\alpha)$ given in* (47) *and depicted in Figure* 19 *(right). The right figure is an example of a finite-element discretization of a meshed chain of* 24 *subdomains.*

TABLE 3

Number of iterations performed by the PSM for the solution of a meshed chain with defined on a squared grid. The bound estimated as $\frac{|\log(Tol)|}{|\log(\rho(\alpha))|}$ is indicated in parentheses.

N	$\alpha = 0.1$	$\alpha = 0.3$	$\alpha = 0.5$	$\alpha = 0.7$
4	164 (190)	58 (79)	35 (62)	30 (131)
9	165 (190)	60 (79)	38 (62)	38 (131)
16	165 (190)	60 (79)	39 (62)	43 (131)
25	165 (190)	60 (79)	40 (62)	45 (131)
36	165 (190)	60 (79)	40 (62)	47 (131)
49	165 (190)	60 (79)	40 (62)	48 (131)
64	165 (190)	60 (79)	40 (62)	49 (131)
81	165 (190)	60 (79)	40 (62)	49 (131)
100	165 (190)	60 (79)	40 (62)	49 (131)

TABLE 4

Number of iterations performed by the PSM for the solution of a meshed chain with a "honeycomb" structure. The bound estimated as $\frac{|\log(Tol)|}{|\log(\rho(\alpha))|}$ is indicated in parentheses.

N	$\alpha = 0.1$	$\alpha = 0.3$	$\alpha = 0.5$	$\alpha = 0.7$
24	82 (190)	42 (79)	31 (48)	29 (48)
36	82 (190)	42 (79)	31 (48)	29 (48)
48	82 (190)	42 (79)	31 (48)	30 (48)
64	82 (190)	42 (79)	31 (48)	30 (48)

the convergence factors do not change and hence the convergence behavior is not affected by the number of subdomains in the chains.

In Tables 3 and 4 we show the number of iterations performed by our numerical experiments. In this case, the similarity of the numerical results obtained with our theoretical estimates is very evident: in Table 3 the number of iterations performed does not decay linearly with respect to α (the overlap) but follows a nonlinear pattern as indicated by our estimate of the contraction factor $\rho(\alpha)$. Notice how the number of iterations performed corresponding to $\alpha = 0.7$ (49) is higher than the one corresponding to $\alpha = 0.5$ (40), as suggested by our estimate of $\rho(\alpha)$ shown in Figure 19. Notice also in Table 4 that the number of performed iterations corresponding to $\alpha = 0.5$ (31) is very similar to the ones corresponding to $\alpha = 0.7$ (30).

6. Conclusions. We considered a two-dimensional version of the physical model presented in [5, 27, 28] for a chain of atoms and proved that the convergence of the

PSM using one atom per subdomain is independent of the number of atoms and thus subdomains. To do so, we first proved some characterization results for the solution to the Laplace equation on the unit disk. Then, using these combined with the maximum principle for harmonic functions, we proved our convergence theorems. Our analysis revealed as a second unexpected result that the Schwarz methods can in this case become slower when one increases the overlap beyond a critical value. Finally, we used our results to estimate the convergence rate of the PSM for the solution of chains of subdomains representing different structures.

REFERENCES

[1] D. Armitage and S. Gardiner, *Classical Potential Theory*, Springer Monogr. Math., Springer, New York, 2000.

[2] V. Barone and M. Cossi, *Quantum calculation of molecular energies and energy gradients in solution by a conductor solvent model*, J. Physical Chemistry A, 102 (1998), pp. 1995–2001.

[3] H. Barucq, M. J. Gander, and Y. Xu, *On the influence of curvature on transmission conditions*, in Domain Decomposition Methods in Science and Engineering XXI, Springer, New York, 2014, pp. 323–331.

[4] T. Betcke, M. J. Gander, and J. Phillips, *Block Jacobi relaxation for plane wave discontinuous galerkin methods*, in Domain Decomposition Methods in Science and Engineering XXI, Springer, 2014, New York, pp. 577–585.

[5] E. Cancès, Y. Maday, and B. Stamm, *Domain decomposition for implicit solvation models*, J. Chemical Physics, 139 (2013), 054111.

[6] G. Ciaramella and M. J. Gander, *Analysis of the parallel Schwarz method for growing chains of fixed-sized subdomains: Part* I, SIAM J. Numer. Anal., 55 (2017), pp. 1330–1356.

[7] P. Ciarlet, *Linear and Nonlinear Functional Analysis with Applications*, SIAM, Philadelphia, 2013.

[8] V. Dolean and M. J. Gander, *Can the discretization modify the performance of Schwarz methods?*, in Domain Decomposition Methods in Science and Engineering XIX, Springer, New York, 2011, pp. 117–124.

[9] L. C. Evans, *Partial Differential Equations*, Grad. Stud. Math., AMS, Providence, RI, 2002.

[10] M. J. Gander, *Optimized Schwarz methods*, SIAM J. Numer. Anal., 44 (2006), pp. 699–731.

[11] M. J. Gander, *On the influence of geometry on optimized Schwarz methods*, SeMA J., 53 (2011), pp. 71–78.

[12] M. J. Gander and S. Hajian, *Block Jacobi for discontinuous Galerkin discretizations: No ordinary Schwarz methods*, in Domain Decomposition Methods in Science and Engineering XXI, Springer, New York, 2014, pp. 305–313.

[13] M. J. Gander and S. Hajian, *Analysis of Schwarz methods for a hybridizable discontinuous galerkin discretization*, SIAM J. Numer. Anal., 53 (2015), pp. 573–597.

[14] M. J. Gander and S. Hajian, *Analysis of Schwarz Methods for a Hybridizable Discontinuous Galerkin Discretization: The Many Subdomain Case*, preprint, arXiv:1603.04073, 2016.

[15] M. J. Gander, L. Halpern, and K. S. Repiquet, *Non shape regular domain decompositions: An analysis using a stable decomposition in* H_0^1, in Domain Decomposition Methods in Science and Engineering XX, Springer, New York, 2013, pp. 485–492.

[16] M. J. Gander, L. Halpern, and K. Santugini, *Continuous analysis of the additive Schwarz method: A stable decomposition in* $H1$ *with explicit constants*, ESAIM Math. Model. Numer. Anal., 49 (2015), pp. 713–740.

[17] M. J. Gander and Y. Xu, *Optimized Schwarz methods for circular domain decompositions with overlap*, SIAM J. Numer. Anal., 52 (2014), pp. 1981–2004.

[18] M. J. Gander and Y. Xu, *Optimized Schwarz method with two-sided transmission conditions in an unsymmetric domain decomposition*, in Domain Decomposition Methods in Science and Engineering XXII, Springer, New York, 2016, pp. 631–639.

[19] M. J. Gander and Y. Xu, *Optimized Schwarz methods with nonoverlapping circular domain decomposition*, Math. Comp., 86 (2017), pp. 637–660.

[20] D. Gilbarg and N. S. Trudinger, *Elliptic Partial Differential Equations of Second Order*, Grundlehren Math. Wiss., Springer-Verlag, Berlin, 1983.

[21] S. Hajian, *An optimized Schwarz algorithm for a discontinuous Galerkin method*, in Domain Decomposition Methods in Science and Engineering XXII, Springer, New York, 2016, pp. 259–266.

[22] P. Henrici, *Applied and Computational Complex Analysis, Volume* 1: *Power Series Integration Conformal Mapping Location of Zero*, Wiley, New York, 1988.
[23] L. V. Kantorovich and V. I. Krylov, *Approximate Methods of Higher Analysis*, Interscience, New York.
[24] A. Klamt and G. Schuurmann, *COSMO: A new approach to dielectric screening in solvents with explicit expressions for the screening energy and its gradient*, J. Chem. Soc., Perkin Trans. 2, (1993), pp. 799–805.
[25] P.-L. Lions, *On the Schwarz alternating method* I, in Proceedings of the First International Symposium on Domain Decomposition Methods for Partial Differential Equations, 1988, pp. 1–42.
[26] P.-L. Lions, *On the Schwarz alternating method* II, in Proceedings of the Second International Conference on Domain Decomposition Methods, 1989, pp. 47–70.
[27] F. Lipparini, G. Scalmani, L. Lagardère, B. Stamm, E. Cancès, Y. Maday, J.-P. Piquemal, M. J. Frisch, and B. Mennucci, *Quantum, classical, and hybrid QM/MM calculations in solution: General implementation of the ddcosmo linear scaling strategy*, J. Chem. Phys., 141 (2014), 184108.
[28] F. Lipparini, B. Stamm, E. Cances, Y. Maday, and B. Mennucci, *Fast domain decomposition algorithm for continuum solvation models: Energy and first derivatives*, J. Chemical Theory Comput., 9 (2013), pp. 3637–3648.
[29] P. J. Olver, *Introduction to Partial Differential Equations*, Springer, New York, 2014.
[30] P. J. Olver, *Complex Analysis and Conformal Mapping*, Lecture notes, University of Minnesota, 2016.
[31] M. M. Peloso, *Classical Spaces of Holomorphic Functions*, Appunti per il corso di Argomenti Avanzati di Analisi Complessa, Milano, 2012.
[32] A. Toselli and O. Widlund, *Domain Decomposition Methods: Algorithms and Theory*, Springer Ser. Comput. Math. 34, Springer, New York, 2005.
[33] T. N. Truong and E. V. Stefanovich, *A new method for incorporating solvent effect into the classical, ab initio molecular orbital and density functional theory frameworks for arbitrary shape cavity*, Chem. Phys. Lett., 240 (1995), pp. 253–260.
[34] Y. Xu, *The influence of domain truncation on the performance of optimized Schwarz methods*, submitted.